The Development of an Acoustic Sensor System to Measure First Year Sea Ice Thickness

by

©Shuo Li

A Thesis submitted to the School of Graduate Studies in partial fulfillment of the requirements for the degree of

Master of Engineering

Faculty of Engineering and Applied Science

Memorial University of Newfoundland

Dec, 2017

St. John's Newfoundland

Abstract

This thesis reports on the development of an acoustic sea ice thickness measurement sensor which has been completed in the Autonomous Ocean System Laboratory (AOSL) of Memorial University (MUN). The development applies acoustic Non-Destructive-Testing (NDT) techniques to test first year sea ice including significant amounts of enclosed impurities (air bubbles and brine pockets). Several single piezoelectric transducers are placed tightly together on a smooth sea ice surface to emit and receive acoustic signals. In addition to showing a detectable reflection from the ice-water interface, the received signal also shows significant energy being reflected from entrained impurities. Based on an assumption of randomly distributed bubbles, the desired reflection from the sea ice-seawater interface can be extracted through sampling the sea-ice in multiple locations. Based on sufficient experimental results, this method has been demonstrated to be feasible and reliable in the lab environment.

Acknowledgements

I first would like to express my sincere thanks to my supervisor, Dr. Ralf Bachmayer, who initially offered this great work opportunity and provides constant professional support. I would also like to thank my lab manager, Neil Riggs, and project manager, Robert Briggs. Neil always gives me expert assistance and encourages me when running into difficulties. Robert has always openly shared with me his technical experience and experiment equipment. I would also like to thank my kind colleagues Jian Cui, Haibing Wang and Stephen Douglas Motty, who have assisted me in doing experiments in the harsh cold reefer. Additionally, I would like to give many thanks to our excellent thermal lab technicians, Matthew Curtis and Craig Mitchell, for their cooperation.

Last, I am deeply grateful to my family, my husband and my two lovely kids. This project could not be completed without their support.

Table of Contents

List of Tables

List of Figures

List of Abbreviations

ADCP	Acoustic Doppler Current Profiler
AMSR-E	Advanced Microwave Scanning Radiometer for Earth Observing System
AOSL	Autonomous Ocean System Laboratory
DFT	Discrete Fourier Transform
DSP	Digital Signal Processing
EM	Electromagnetic-Inductive
IPS4	Ice Profiler
FT	Fourier Transform
MUN	Memorial University of Newfoundland
NC	Normally-Close
NDT	Non-Destructive-Testing
NO	Normal-Open
PE	Pulse-Echo
STFT	Short Time Fourier Transform
TGC	Time Gain Compensation
TT	Trough-Transmission
ULS	Upward Looking Sonar

Chapter 1

Introduction

1.1 Motivation

Sea ice is a significant component of the Arctic coastal environment. It is closely related to many human activities performed in Arctic areas such as resource extraction and shipping. Particularly for the northern peoples who have been living in this harsh environment for many centuries, sea ice is an integral part of their lives. To maintain a sufficient food supply during the winter, they need to hunt and travel across sea ice, which comes with certain risks. Recently, due to changes in the Arctic climate, the sea ice extent has been declining sharply year after year. According to the Advanced Microwave Scanning Radiometer for Earth Observing System (AMSR-E) record, the minimum ice edge tested in September has decreased from the red area (Fig.1.1) to the white area over 1970-2007. Before 1996, it had gently declined -2.2 to -3.0% per decade (Fig.1.2), but since 1996 the trend has accelerated to -10.1 to -10.7% per decade [3]. Therefore, finding safe travel routes based on past climate conditions or sea ice records has become less reliable. For those Northern communities, the safety issue has become their primary concern. A survey made by the Nain Research Centre

indicates that around one-half of traditional travel routes cannot be used, and the unpredictable ice situation has made more than 68% people afraid to travel on ice [17].

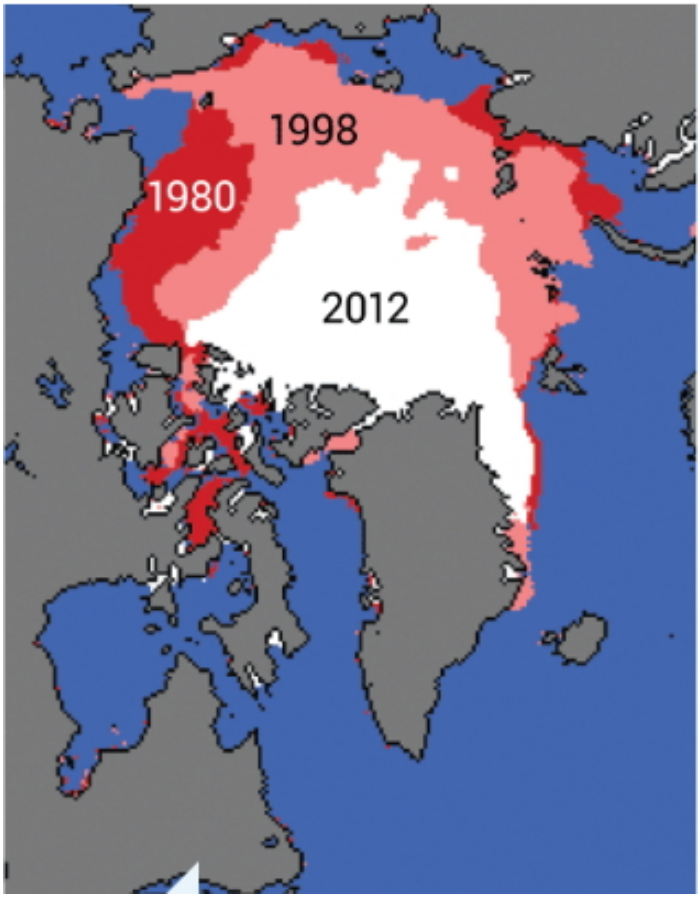

Figure 1.1: Comparison of sea ice extent from 1978 (red area) to 2012 (white area) [2]

Sea ice bearing capacity is mainly determined by thickness, which is a very important parameter when deciding how much load an ice sheet can support and what kind of human activity can be operated on it safely. The sensor system designed in this thesis is a user-friendly device that can be used to monitor the sea ice situation. It will measure and record the current sea ice thickness on a computer. In the future, it may send test results to a server directly in real time by satellite. Knowing the present sea ice situation will help people make better travel route plans or will assist

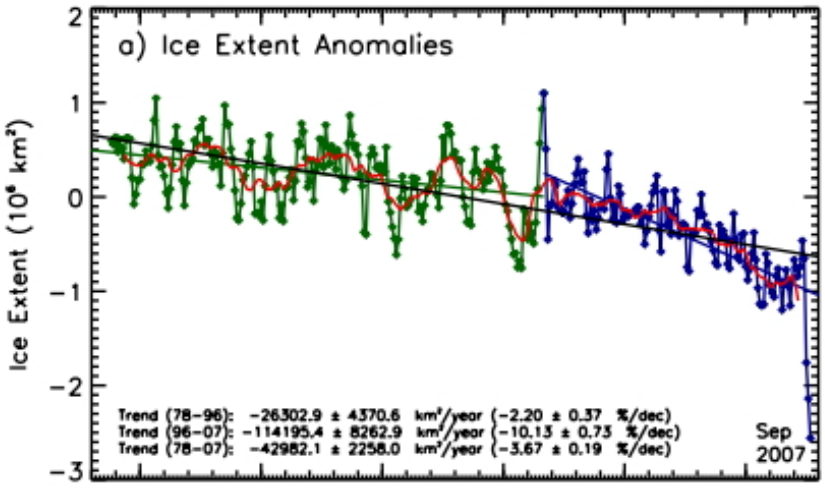

Figure 1.2: Trend of sea ice extent [3]

people in deciding on safe travel routes.

1.2 Problem Statement

The reason the acoustic method can be applied in thickness measurement is because different materials have different acoustic impedances. Similar to light, once an acoustic wave reaches an interface, where there are two media having different acoustic impedances located on both sides of it, the acoustic wave will change its original travel direction and split into two parts; the one transmitted to the lower medium and the other one reflected to the top surface of the upper medium. More details are introduced in the next section. The transmission/reflection ratio is determined by the amount of mismatch of their impedances [7]. In this project, the boundary that needs to be detected is the sea ice/seawater interface. What is interesting is that sea ice and seawater cannot be simply identified as two different materials; in other words, they are two phases of the same matter. Therefore, their acoustic impedances are very close to each other. Unfortunately, this fact highly increases the degree of difficulty of this project. Due to the small mismatch in acoustic impedance between seawater

and sea ice, most energy is transmitted into the seawater below the ice layer, and only a small part is reflected. Another two big issues faced in this project are entrained air bubbles and brine pockets (in the remainder of the thesis referred to as impurities) which are both better reflectors than seawater. As Fig.1.3 shows, when using an acoustic method to measure thickness, two identical transducers are required. One works as a pulser to generate an acoustic signal, and another one works as a receiver to collect reflected signals. From this figure it also can be observed that in the sea ice thickness measurement, before receiving the reflection from the bottom surface, the receiver may already detect a few stronger air bubble reflections, which add more noise and can make the bottom surface reflection inconspicuous.

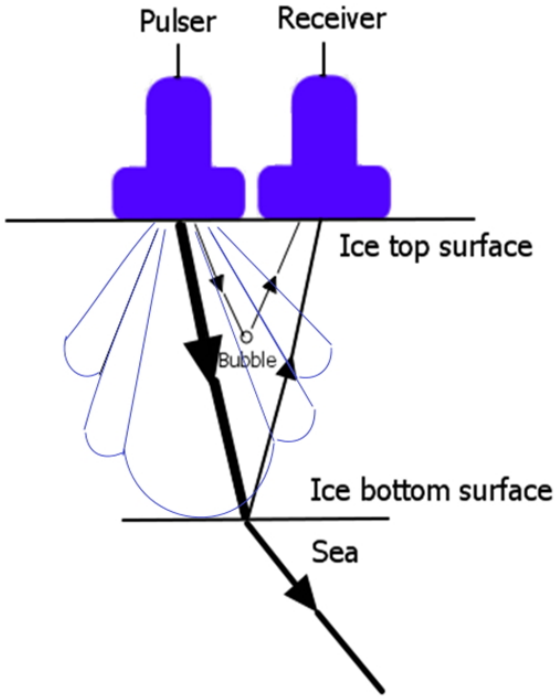

Figure 1.3: Acoustic propagation in sea ice

Based on the random distribution of impurities and the fixed position of the bottom interface reflection, by observing a set of measurements collected from multi-locations

then the time containing the highest amount of reflections can be recognized as that of the bottom reflection. However, this method brings new questions that have to be answered through sufficient experiments: what is the minimum number of positions needed to detect the bottom surface successfully and what are suitable arrangements for transmitter-receiver locations. Additionally, an acoustic wave has high attenuation in air; thus, to avoid any unnecessary energy loss, an appropriate couplant should be applied between the transducer and sea ice to achieve better contact. Considering the harsh Arctic environment, this sensor is required to work in $-30°$C to $-50°$C. To investigate a proper couplant that has a low freezing point, better transmission, and is water insoluble is another important objective.

1.3 Technologies for Sea Ice Thickness Measurement

With the recent increasing interest in sea ice, several techniques have been applied to observe sea ice growth. The earliest method which is also the simplest one, is to use a hand drill. Although this traditional method can provide accurate, reliable test results, the operation requires a person on the ice, representing a potential risk. Upward looking sonar and electromagnetic-inductive technology (EM) are two other popular approaches used in sea ice thickness measurement. The following sub-sections introduce these two methods in details.

1.3.1 Upward Looking Sonar

Moored Upward looking sonar (ULS), which was developed a few decades ago, is another widely used method in this research area. Before the ice season approaches, a pair of an ice profiler (IPS4) and a current profiling acoustic instrument are deployed

on the seabed [4][18] as shown in Fig.1.4.

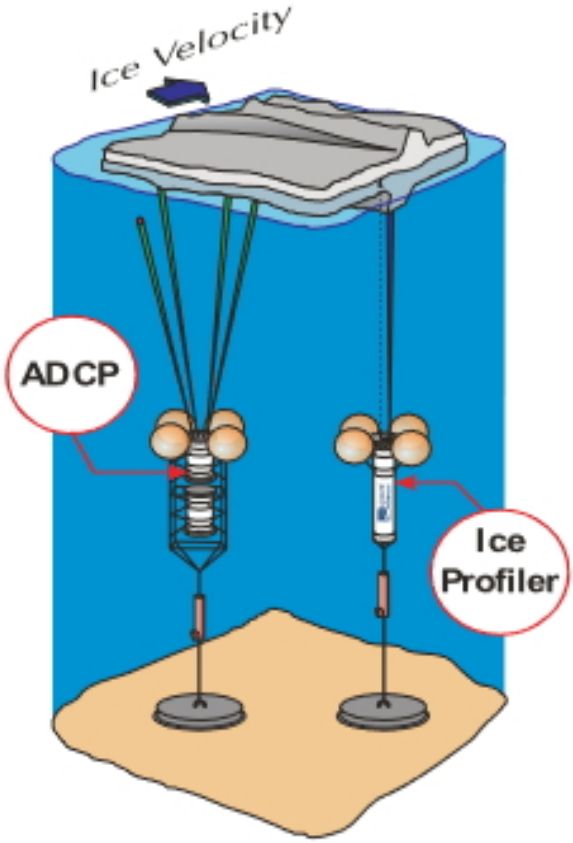

Figure 1.4: Upward looking sonar [4]

In IPS4, there is a built-in sounder which can generate high frequency acoustic wave to monitor a portion of sea ice underface over time series. At the meantime, it records the hydrostatic pressure, P_{btm}, atmospheric pressure, P_{atm}, and tilt angle, θ, as well which are significant parameters to derive accurate ice draft, d, by using following two equations.

$$d = \eta - \beta r cos\theta \tag{1.1}$$

$$\eta = (P_{btm} - P_{atm})/\rho g - \Delta D \tag{1.2}$$

where η is acoustic sensor depth, β is a factor accounting for changes over time in the mean sound speed in the upper water column, ΔD is the vertical distance between acoustic and hydrostatic sensors, ρ is the density of seawater and g is the acceleration of gravity.

Although this ULS works well in sea ice investigation, it has two serious disadvantages: real time data access and site adjustment. Not all the recorded data can be easily sent from underwater and since the whole system has been mounted it cannot be moved until next spring.

1.3.2 Electromagnetic-inductive Technology

Recently, electromagnetic-inductive technology has been applied in determining sea ice thickness as well. Each such instrument has a transmitter coil and a receiver coil deployed at a certain distance from each other. Comparing with the seawater, whose electrical conductivity is between 2300 mS/m to 2900mS/m, the conductivity of sea ice is negligible. Due to this large contrast, eddy currents will be generated under the seawater by the low frequency EM field which is caused by the transmitter coil. Consequently, the receiver coil will detect a secondary field produced by this current. Through observing the ratio of the secondary-to-primary field σ_a, which is only dependent on the distance between the instrument and sea surface, then sea ice thickness can be derived [19]. For different investigative purposes and areas, an EM instrument can be mounted on a sea ice surface, ship or helicopter [5].

For ground-based measurements, an EM instrument is placed on the sea ice surface directly in a vertical orientation. Therefore, the two coils function as horizontal

magnetic dipole antennas (HMD). Then ice thickness z_i is derived from Eq.1.3. In this equation, d_{EM} is the distance between the system and sea surface as determined by EM instrument, and d_{Instr} is the height of the instrument.

$$z_i = d_{EM} - d_{Instru} \tag{1.3}$$

For ship-based measurements, the instrument is deployed at the end of an ice breaker as shown in Fig.1.5. For large area estimation, an EM instrument will be mounted below a helicopter or in a fixed-wing airplane as shown in Fig.1.6. While using these two methods, the EM instrument can be operated either vertically to work in horizontal magnetic dipole mode (HMD) or horizontally to work in vertical magnetic dipole mode (VMD). In Fig.1.5 and Fig.1.6, both instruments are deployed horizontally and performed in VMD mode to achieve better penetration. In addition, to get the height of instrument above the sea ice surface which is labelled as d_{Laser} in Fig.1.7, a laser altimeter is integrated under the bottom of the EM instrument. Then the ice thickness can be obtained from Eq.1.4.

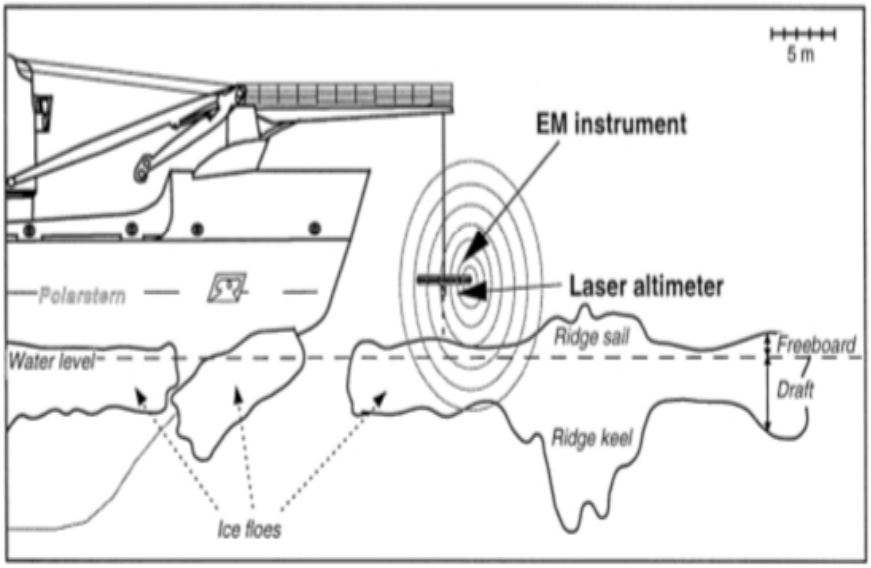

Figure 1.5: Ship-based electromagnetic-inductive instrument [5]

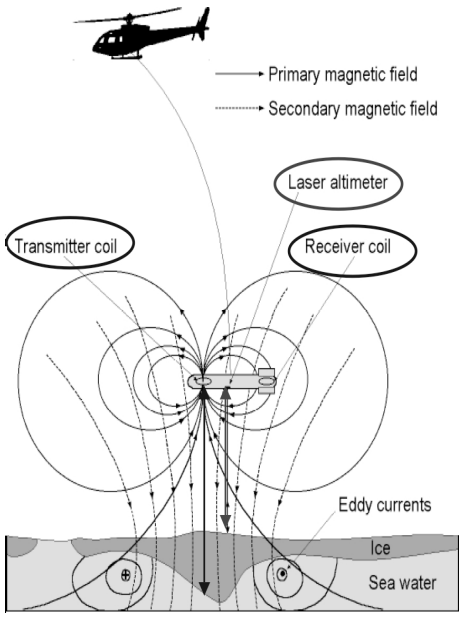

Figure 1.6: Airborne electromagnetic-inductive instrument [6]

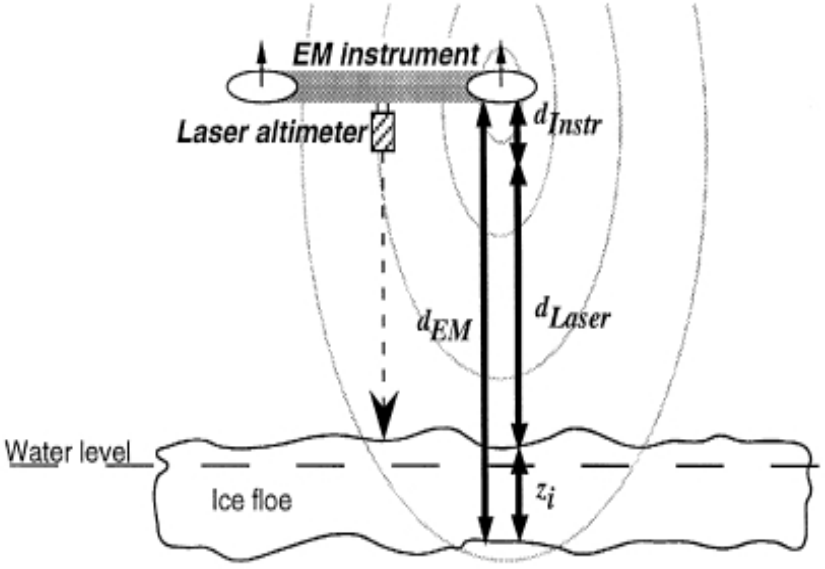

Figure 1.7: Principle of using EM to measure sea ice thickness [5]

$$z_i = d_{EM} - d_{Instru} - d_{Laser} \tag{1.4}$$

Since the response of EM is not a point measurement but an area of a footprint, whose

diameter is on the order of two to three times that of the instrument height above the sea surface, so this method has very poor result in point and small area measurement. It is more effective in estimating the mean thickness of a large area.

1.4 Outline of the Thesis

This thesis is composed of six chapters which outline the development and testing of a new acoustic sensor system to measure sea ice thickness, concluding with a perspective of future work.

In Chapter 1, the author provides the motivation behind the design of the ice thickness measurement system in the first section, and discusses the challenges of this project in the following section. A few widely used techniques in sea ice thickness measurements are reviewed in the third part. After this, the structure of the thesis is introduced.

In Chapter 2 the author reviews the basic principles of ultrasonic measurements and the relevant properties of sea-ice.

Chapter 3 consists of two main parts. In the first part, the author describes the design conception of the proposed sensor system and explains each component in detail. The experiment set up and operation procedure are introduced in the second part.

An algorithm to process the acoustic data was developed in the Matlab environment. In Chapter 4, this approach is explained step-by-step and intermediate results are illustrated.

In Chapter 5 experimental results are presented. Results consist of raw and processed measurements taken from different ice samples. The results are interpreted based on the measurements and used to draw conclusions about the measurement process.

Chapter 6 concludes this thesis by summarizing the achievements and providing an outlook towards future work.

Chapter 2

Theoretical Background

2.1 Physics of Ultrasound

2.1.1 Wave Propagation

Sound which has frequency higher than 20 kHz is beyond human hearing range and is called ultrasound [7]. Its propagation wave, mainly relying on the movement of medium particles, can be divided into two principle categories according to different wave propagation directions: a longitudinal wave and a shear wave. In longitude waves, medium particles oscillate in the same direction as that of wave propagation. In shear waves, in contrast, particles oscillate transverse to the propagation direction. All experiments in this project use a direct contact transducer which is a kind of single element longitudinal wave transducer. Therefore, all the acoustic parameters used in the rest of this thesis refer to longitudinal waves.

2.1.2 Wave Length, Frequency and Velocity

Wave length, frequency and velocity are three principle properties of acoustic waves. Their relationship can be described by Eq.2.1, where λ is wavelength, v is acoustic propagation velocity, and f is frequency in Hertz.

$$\lambda = \frac{v}{f} \tag{2.1}$$

According to the above equation, it can be observed that wavelength is proportional to velocity and inversely proportional to frequency. Velocity is mainly determined by the medium of propagation. Frequency is an inherent property of the object producing the ultrasonic wave. Therefore, wavelengths will vary in different media. It is important to know the wavelength, since any discontinuity, such as a flaw in the material, whose diameter is larger than a half wavelength may block the propagation path and reflect part of the energy back to the receiver.

2.1.3 Acoustic Impedance

Acoustic impedance (Z), which is used to indicate how much resistance the ultrasound beam encounters while it travels through a medium, is a significant physical property of a material [7]. It is defined as the product of the density of the material (ρ) and acoustic velocity (v) as shown in Eq.2.2. This parameter is important in determining the reflection/transmission ratio, which is introduced in the next section.

$$Z = \rho v \tag{2.2}$$

2.1.4 Reflection and Transmission Coefficients

Similar to the propagation of light, when an acoustic wave reaches an interface that contains an impedance mismatch between the materials located at both sides of the boundary, a portion of the energy will be reflected, and remaining energy will be transmitted to a lower medium as displayed by Fig.2.1.

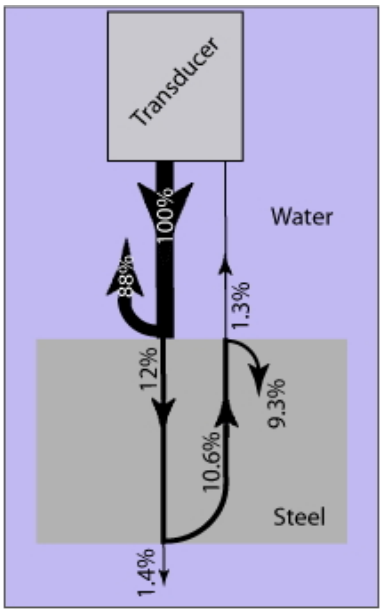

Figure 2.1: Propagation between two media [7]

The amount of impedance mismatch determines the percentage of reflected energy; in other words, a greater mismatch causes a greater percentage of energy reflected from the boundary. With the known acoustic impedances of those two materials (Z_1 and Z_2) obtained from Eq.2.2, the fraction of reflected energy can be computed using Eq.2.3. This value is known as the reflection coefficient. With the reflection coefficient known, the transmission coefficient can easily be computed as T=1-R, where use math mode.

$$R = \left(\frac{Z_2 - Z_1}{Z_2 + Z_1}\right)^2 \tag{2.3}$$

2.2 Properties of First Year Sea Ice

2.2.1 Sea Ice Formation

The process of sea ice formation is very different from and more complicated than fresh water ice formation. In fresh water, when the air temperature drops down to 0°C or below, then the surface will quickly form a thin ice layer with lesser density thus floating on the water. While the temperature remains below freezing, this ice layer will continue to grow in depth. Similar to a layer of insulation, the fresh water ice cover keeps the deeper water from cooling so that fish can survive in deep enough water. But in seawater, as the top layer is cooled by the cold air temperature it becomes denser and sinks until it reaches the lower layer, which has the same density. In the meantime, warmer or less saline water rises to form a new surface layer which will experience the same cooling down and sinking process [20]. The mixing process is carried out continually until the upper 10-20 meters of seawater is cooled, then the ice freezing process starts. At the onset of freezing, small ice crystals form a slushy layer called frazil ice, and then these crystals cluster together and become small rounded pieces of ice called pancake ice. After a while, young ice, which is a thin, stable ice layer, covers the sea surface. As long as the surrounding air temperature remains lower than -1.80°C which is the general freezing point of seawater, a thin ice layer continues to grow from the bottom surface progressively and forms solid first year ice. The various pictures in Fig.2.2 display sea ice at different stages.

2.2.2 Sea Ice Structure

As seawater freezes, most inherent salt is expelled to the surrounding seawater, but a small amount is trapped in the space between ice crystals either in a solid or liquid state called a brine pocket. Similar to the formation of a brine pocket, an air pocket

(a) Frazil Ice

(b) Pancake Ice

(c) Young Ice

(d) First Year Ice

Figure 2.2: Sea ice at different stages [8][9]

can be formed by trapped air bubbles. The amount of brine and air bubbles is influenced by multiple environmental factors including freezing speed, seawater salinity and temperature [21]. These two elements, especially air bubbles, not only create obstacles to sound propagation but also introduce an additional level of complexity to the measurement of sea ice thickness.

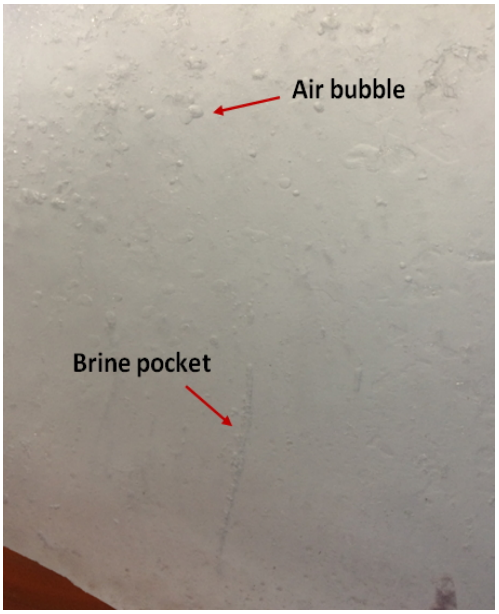

Figure 2.3: Brine pocket and air bubbles in laboratory made sea ice

2.2.3 Physical Properties of First Year Sea Ice

The following table displays some rough estimated values of the physical properties of first year ice whose default salinity and temperature are 3.5‰ and $-5°$C. These characters can be various in different environments.

Table 2.1: Physical properties of first year sea ice [1]

Density(of solid phase)	$900kg/m^3$
Melting point	-1.80°C
Specific heat	$8kJ/kg/$°C
Latent heat of fusion(or melt)	$280kJ/kg$
Thermal conductivity	$2.1W/m/$°C
Acoustic velocity(Longitude wave)	3400-3600m/s

2.3 Measuring Thickness Using Ultrasound

Due to the reflection property of ultrasound mentioned in Section 2.1.4, ultrasound has been widely used in Non-destructive testing to measure element thickness and detect internal flaws. Based on the time taken for an ultrasonic wave to return to the surface and the speed of sound in this kind of medium, then the desired result can be calculated by using a simple equation Eq.2.4, where v is sound speed, t is propagation time and d is round trip distance (twice the thickness).

$$d = v \times t \tag{2.4}$$

Fig.2.4 shows an example using ultrasound to measure the thickness of an aluminium block with a height of 15 cm. There are two identical acoustic sensors placed on the top surface: one is responsible for generating an ultrasonic signal, another one is used to receive a reflected signal.

Fig.2.5 displays an original received return signal. In this figure, the x-axis is the sampling point, which is easy to exchange with time by dividing the sampling frequency,

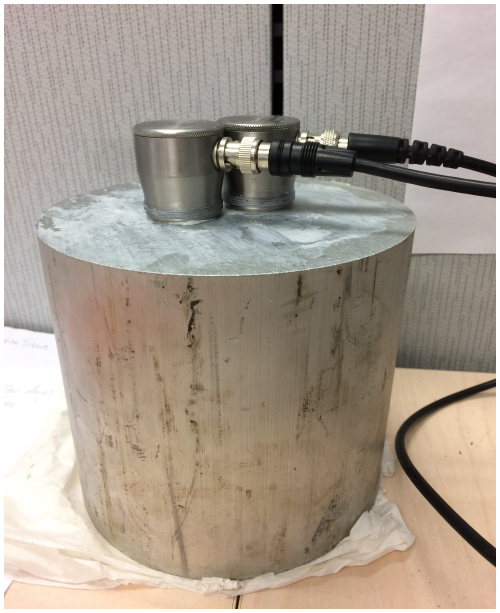

Figure 2.4: Using acoustic to measure the thickness of aluminium block

fs, and the y-axis is signal power, represented by the percentage of the original emitting power. There are a few detected strong pulses and each one covers a number of sampling points, but only the time when the power of each pulse reaches its maximum value is recognised as the correct time that indicates reception of a return signal. Therefore, after using the Short Time Fourier Transform (STFT) and some other data processing steps which are introduced in later chapters, then the power curve shown in Fig.2.6 is obtained. In this figure, x-axis represents time(s) and y-axis represents the power density(W/Hz). From this figure, it can be seen that the first and also the strongest reflection appears at 47 ns. Multiplying it with the speed of sound in aluminium, 6320 m/s, a travel distance of 29.7 cm can be calculated, and the measured thickness, 14.85 cm, which is equal to half the travel distance, can be known as well. The other two reflections occurring at integer numbers of the first travel time are caused by the subsequent transmits through the block and their reflections.

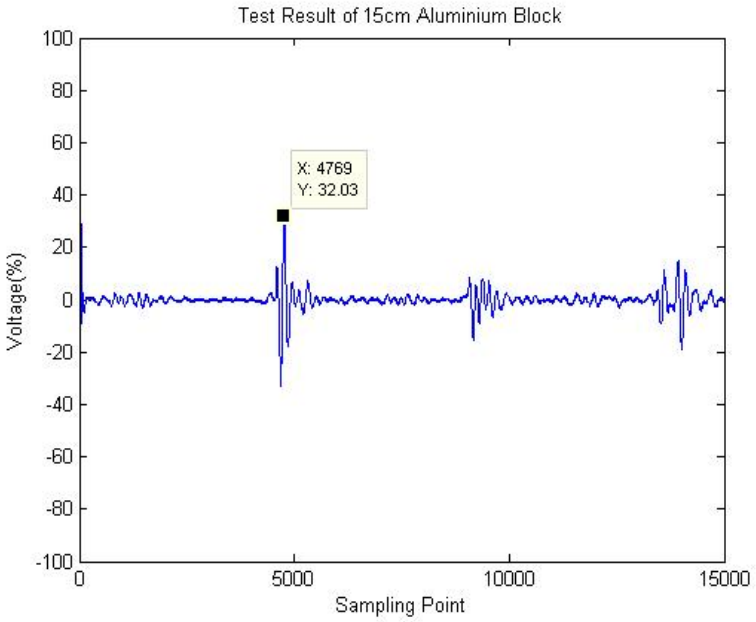

Figure 2.5: Test result of 15 cm aluminium block

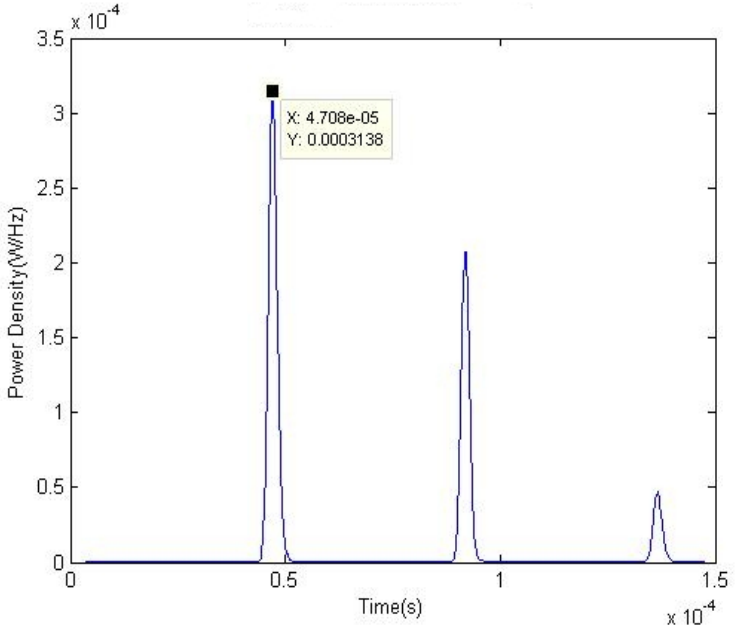

Figure 2.6: Power curve of aluminium test

Chapter 3

System Design and Experiments

3.1 System Overview

An automatic sensor system which is responsible for collecting and saving test results regularly for the long term is composed of four main components: a set of identical transducers, channel selector, transducer processor and system controller as shown in Fig.3.1. In this system, all transducers are controlled by a transducer processor, and each of them can work as a pulser to generate an acoustic signal or a receiver to collect the reflected signal. The channel selector controls the working sequence of those transducers to ensure that only one pair of adjacent transducers work at any one time. OPBOX is a transducer processor manufactured by OPTEL, a company in Poland. OPBOX keeps listening for a timing signal sent by the system controller, and once this signal is detected as positive then OPBOX gives an electrical pulse from its inherent circuit to the transducer to trigger it, and at the same time, it turns on its receiver circuit connected with another transducer to collect and pass the return signal to the system controller. This timing signal is also sent to the channel selector at the same time so that it can work with the transducer processor synchronously

to collect signals from different pair of transducers placed at multi-locations. In the initial stage, a PC laptop is used as a system controller to monitor the timing signal and record all test data, but in the future it will be replaced by a micro-controller.

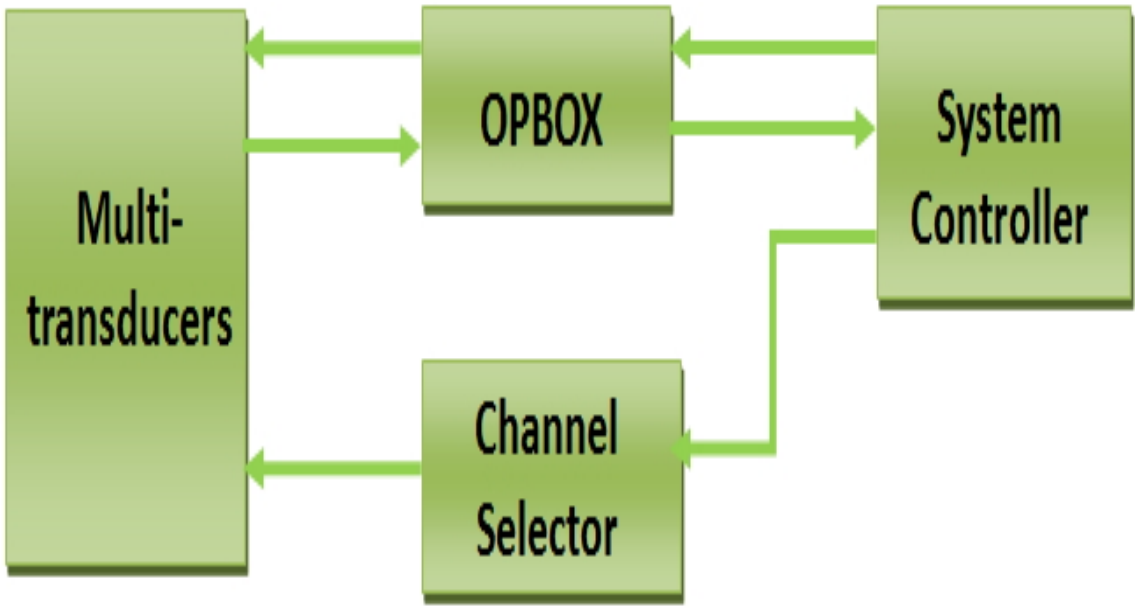

Figure 3.1: System overview

Fig.3.2 shows a flow chart which describes how this system works. Assume it is asked to do a test twice per day every 8 am and 8 pm for 50 days, this means it has to work 100 times in total. After the system starts, it continually monitors the time, and once it reaches the working time the user has set, it will go to the next step, checking how many tests it already did. If it is 100 times then the system stops working; otherwise, it triggers the channel selector and OPBOX. These two pieces of equipment work cooperatively to collect data from different pairs of transducers and record data to a connected computer. Once data collection is done, the system goes to sleep and waits to execute the next test.

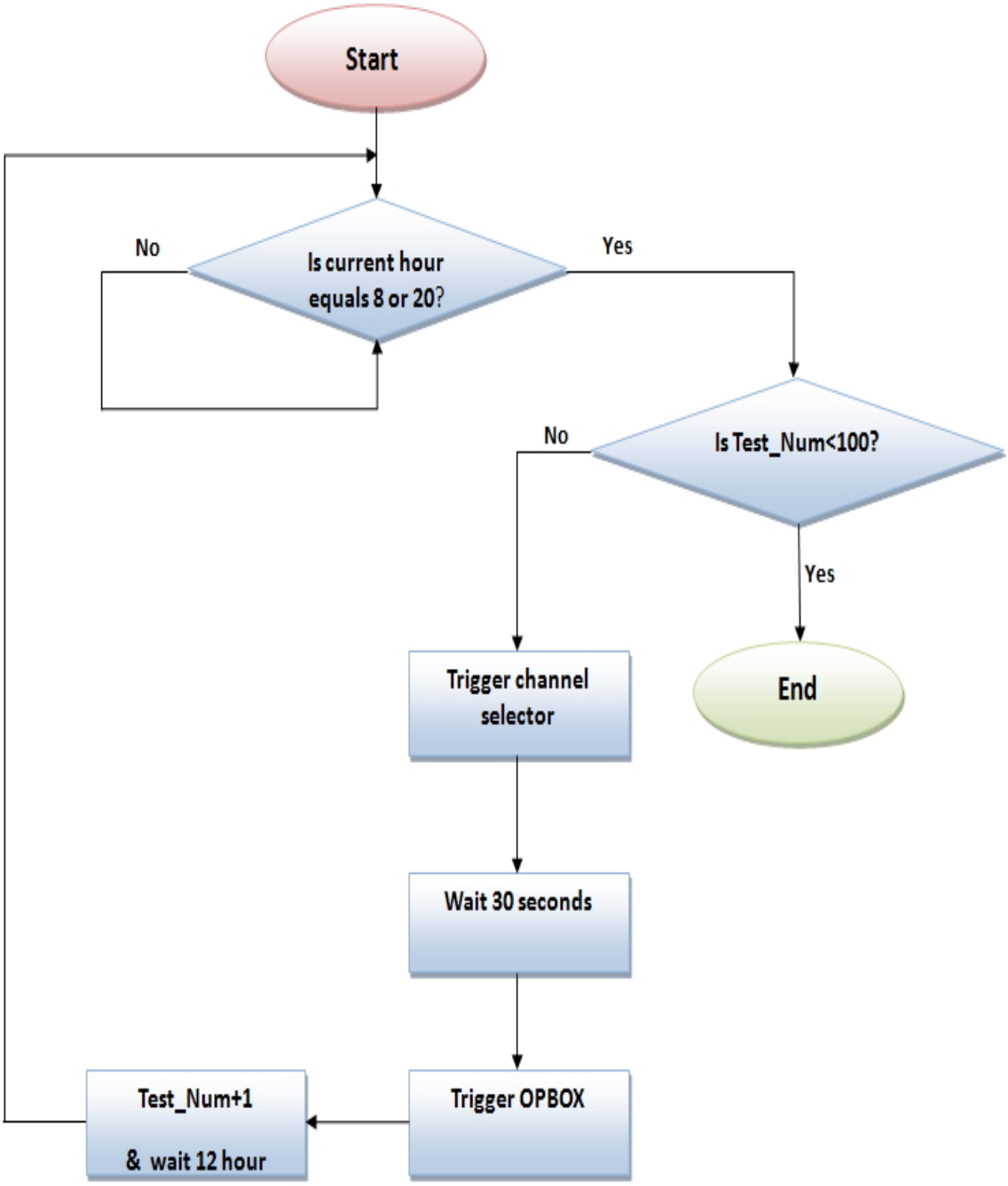

Figure 3.2: System flow chart

3.2 Transducer

3.2.1 Piezoelectric Transducers

The principle of an acoustic transducer is based on converting an electrical pulse to a mechanical vibration, and vice versa. This unique physical property is provided by the heart of each transducer, a piezoelectric ceramic element whose size and shape determine the intrinsic frequency of this transducer [7]. In this project, by comparing the performances of 500 kHz and 250 kHz transducers in low temperature environment, and considering the size of inherent air bubbles, the 250 kHz piezoelectric transducer which has larger wavelength is selected and applied in all following experiments. Further, the author selected to use the product from Sonatest Inc. All its dimensions are displayed in Fig.3.3.

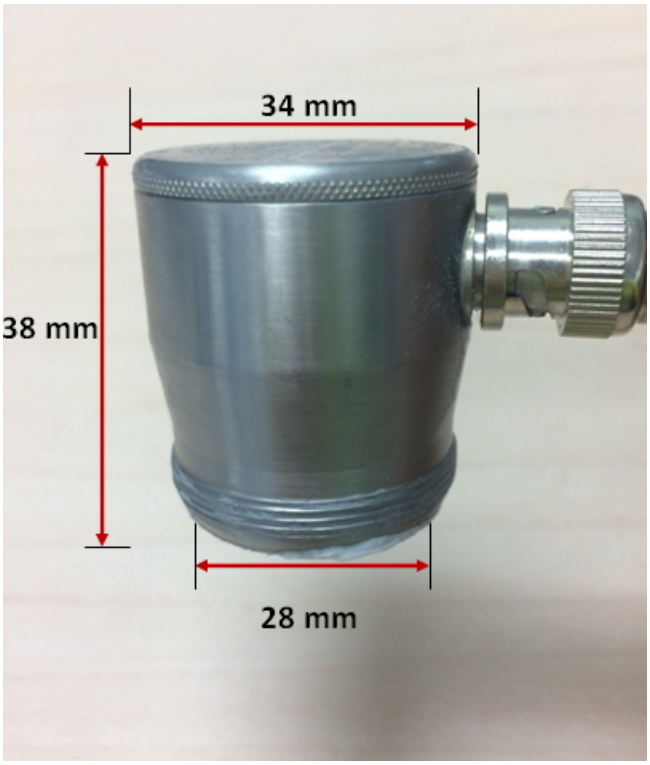

Figure 3.3: 250KHz transducer dimensions

3.2.2 Near/Far Point

The sound field of each transducer can be divided into two parts: the near field and far field. The demarcation point of these fields is called the near/far point, distance N of where to the transducer, is a significant parameter that must be known before choosing a transducer. This is because, in the near field, the wave is not fully stabilized, and only the part beyond it forms a uniform wave that can be used in an ultrasonic test [7]. Furthermore, in the far field, the beam spreads out in a pattern originating from the center of the transducer. For the above reasons, it is concluded that reliable results should be detected in the far field area. The Near/far point distance, N, is a function of the diameter of the active piezoelectric element, D, speed of sound in test material, c, and transducer frequency, f, shown as Eq.3.1.

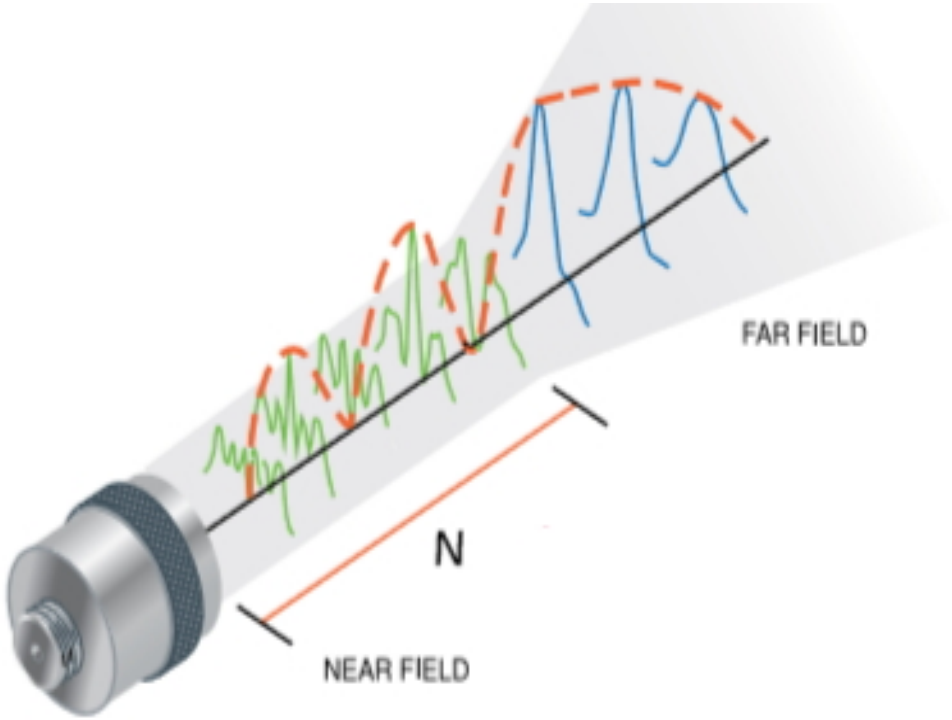

Figure 3.4: Near/far point [10]

$$N = \frac{D^2 f}{4c} \tag{3.1}$$

Through some investigation and evaluation, the Sonatest PSLF250 displayed in Fig.3.3, whose piezoelectric ceramic element diameter is 28 mm, and frequency is 250 KHz, is selected to be applied in all experiments. By using Eq.3.1 with the minimum sound speed, 3400 m/s, then the maximum near/far point distance of this transducer is 14.4mm. Therefore it is suitable for testing the sea ice thicker than this value.

3.2.3 Beam Spread Angle

Beam spread is another parameter that must be considered before performing ultrasonic test. As in the definition cited from the NDT resource center [7], it is a measure of the whole angle from side ($-3dB$) to side of the main lobe of the sound beam in the far field as shown in Fig.3.5. It is inversely proportional to the penetration ability of the ultrasonic wave. When more energy scatters on a wide area, then less energy remains at the center where the power is concentrated upon penetration. On the other hand, in the sea ice test, due to the interference of air bubbles and brine pockets, a greater beam spread angle means more propagation paths. To achieve the best results, two aspects, beam spread angle and penetration ability, must be considered at the same time.

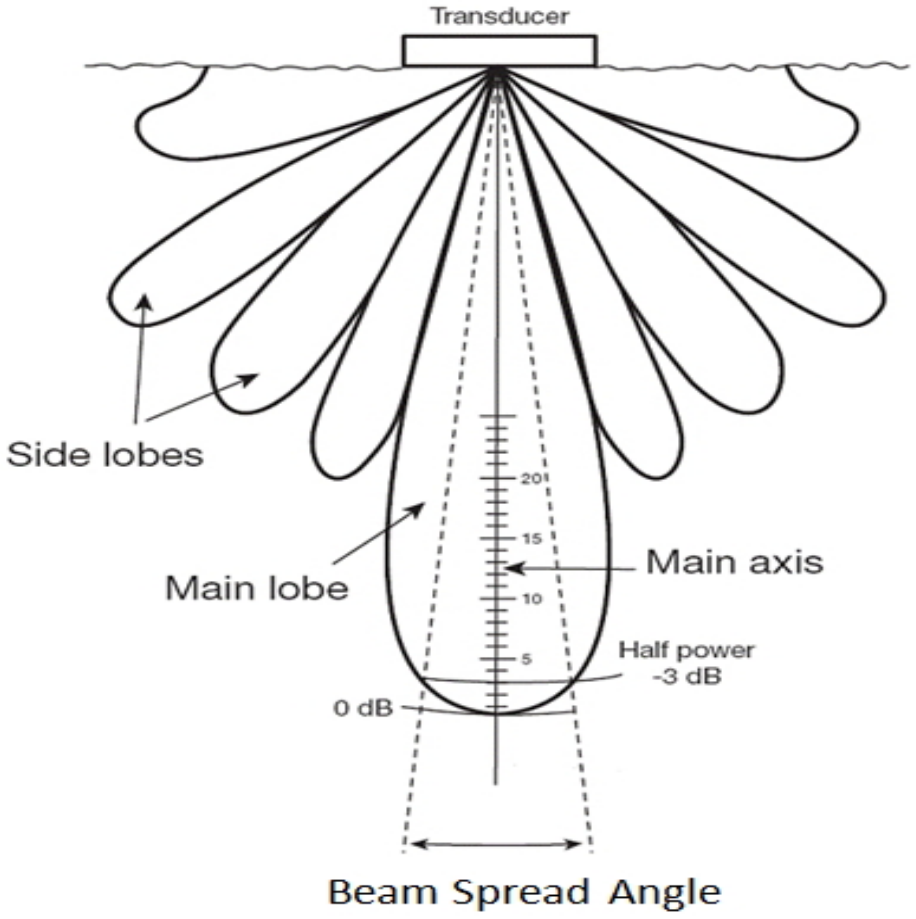

Figure 3.5: Beam spread angle of transducer [11]

The beam spread angle is decided by the sound velocity, transducer frequency and active element size. Their relationship is displayed as Eq.3.2, where θ represents the beam spread angle, V represents the sound velocity in the medium, D represents the diameter of transducer and F represents the frequency of the transducer. According to this equation, the beam spread angle of the Sonatest PSLF250 selected for this project is around 8 degrees.

$$sin\frac{\theta}{2} = 1.2\frac{V}{DF} \tag{3.2}$$

3.2.4 Transducer Testing Mode

In non-destructive acoustic testing, two common approaches are used [22]: (a) PE (Pulse-Echo) method; and (b) Through-Transmission (TT) method. In the PE method the transmitter and receiver are placed on the same side of the test specimen. The echoed signal is analysed in order to detect reflections from any discontinuities within the examined specimen. Initially, a transmission pulse with a minimal length of several wavelengths is transmitted into the material. The minimum length is determined by the detection limits of the acoustic processing methods. Based on the material thickness, the speed of sound and the pulse length, it can be determined if a method can use a single transducer or a pair of separate transducer and receiver. If the length of the transmit pulse is short compared to the material thickness one can potentially use a single transmitter-receiver (Transceiver) device (see panel (a) in Fig.3.6) by turning off the transmitting function after the transmission is completed and enabling the receiving function. In case the transmit pulse length approaches the length of twice the sample thickness, i.e. the total transmission path, two separate transducers are used in a transmitter-receiver pair (see panel (b) in Fig.3.6). The TT-mode always requires people to put two separate transducers on the different sides of test specimen. The amplitude of the received signal is analysed in order to detect any anomalies in the path of the transmission. As demonstrated above, in this project, there is only one side of sea ice exposed to people to place transducers, so the PE method is more suitable.

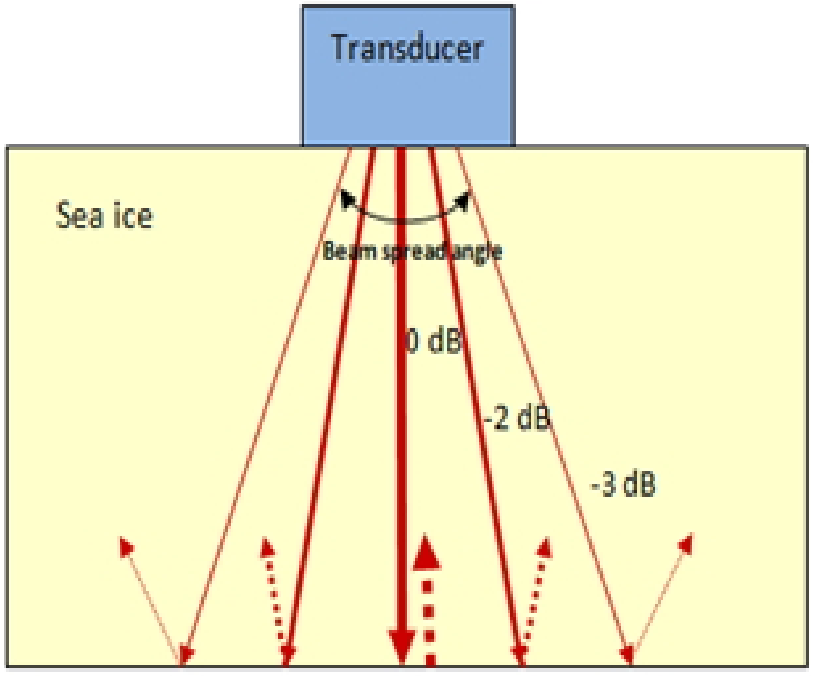

(a) Single Mode

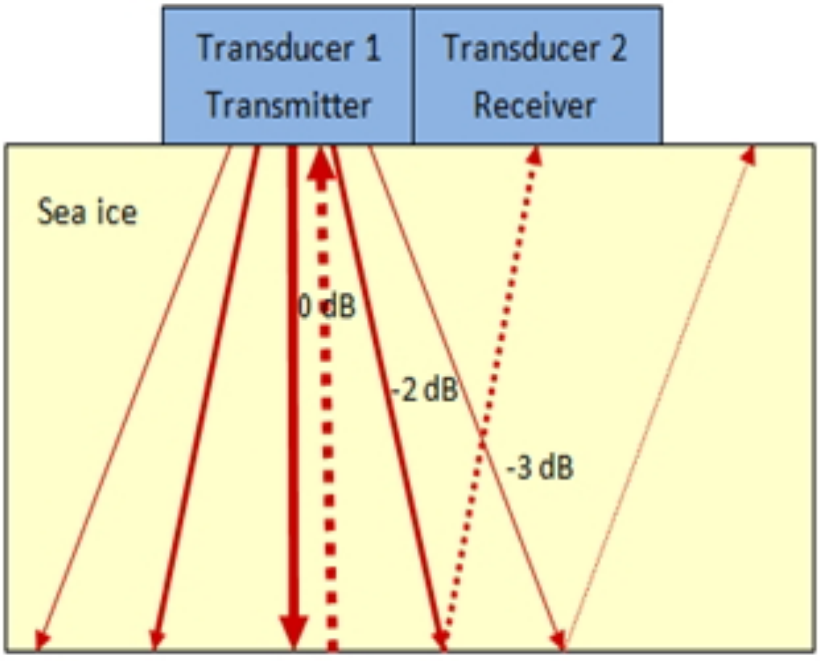

(b) Separate Mode

Figure 3.6: Transducer testing mode in Pulse-Echo (PE) method

As described above, the PE method can be implemented by two modes, using one single transducer or two separate transducers. In the single mode, the energy reflected from the ice – water interface is incident from the center of the beam, where most of the emitted energy is concentrated as displayed in Fig.3.6a. In this figure, the weight of the red arrow represents the amount of energy. From Fig.3.6b, we can observe that, while using two transducers, the energy reflected back to the receiving transducer is from the side of the transmitted beam where the energy is less intense. Therefore, in terms of penetration ability, the single mode is a better choice; however, it does not perform well at temperatures below 0°C. This is because the piezoelectric ceramic element of the transducer generates mechanical vibrations not only from its bottom part, which contacts the test medium tightly, but also from its top part as well. An acoustic signal generated by top part vibration will propagate down through the piezoelectric ceramic element and be reflected by its bottom surface. In a normal temperature environment, by using a special technique developed by transducer manufacture this internal reflection can be reduced to an undetectable level, but in a harsh, cold environment this technique does not work well. Due to the large acoustic impedance mismatch between piezoelectric ceramic element and sea ice, most energy of this internal noise will be reflected up and become non-ignorable. Sometimes it is even too strong to overwhelm useful information. But on the other hand, only a tiny part of this noise will be transmitted into the sea ice. And this small amount will be exhausted during the propagation. Thus, while using two separate transducers, this internal noise caused by the emitter will not be detected by the receiver and will not affect the test result. Therefore, two transducers mode works better in this project. The following two figures show the same conclusion. Fig.3.7a and Fig.3.7b display the comparisons of a special signal called an "empty signal" by the author. It is obtained through hanging transducers in the air without touching any other material. This

method can be used to evaluate the internal interference generated by the processor and transducers. From these two figures, it can be observed that using the two separate transducers mode is much more suitable for a low temperature environment.

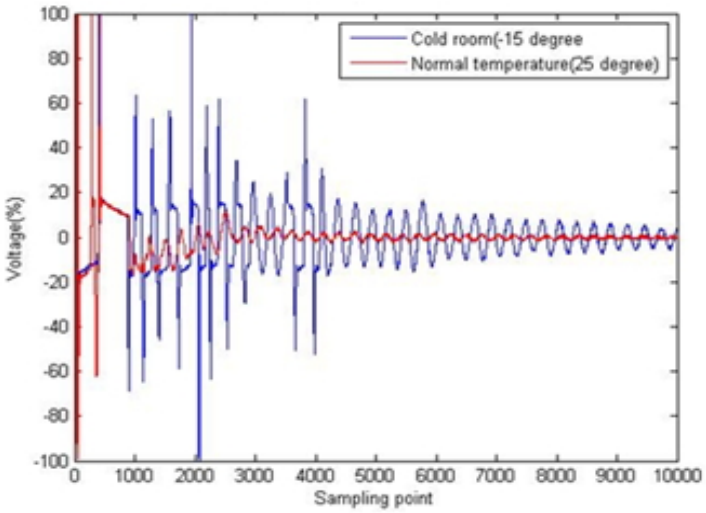

(a) Comparison of "empty signal" tested in different environment with single transducer

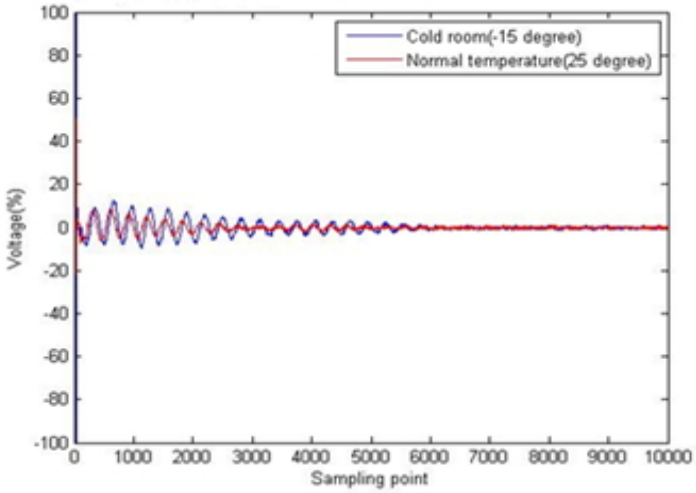

(b) Comparison of "empty signal" tested in different environments with two separate transducers

Figure 3.7: Influence of temperature in different testing modes

3.3 Transducer Processor

3.3.1 OPBOX

The transducer processor, OPBOX ver 2.0, designed and manufactured by OPTEL company [12], is a complete ultrasonic testing device integrated with a pulser and receiver. All its dimensions are displayed in Fig.3.8.

Figure 3.8: OPBOX dimensions [12]

It contains four input/output connectors. Two female BNC connectors are located on the same side, labelled as PE and TT. The PE port can perform receiving and emitting functions in turn, but the TT one only can collect the returning signal. On the other side, there are one DB15 female connector, which is not used in this project, and one USB connector. The USB connector is not only responsible for the power supply, but also is in charge of communication with the computer and data transmission. The inside structure of the OPBOX is shown in Fig. 3.9. According to this diagram, it can be observed that the selection of the receiving port is determined by the switch in front of the receiver block. Furthermore, there is a switchable built-in filter. In order to record all potential information, this analog filter is kept turned off in all experiments and replaced by a digital filter which is designed by Matlab and

applied for the later data processing step. Some significant features of the OPBOX are displayed in Table 3.1.

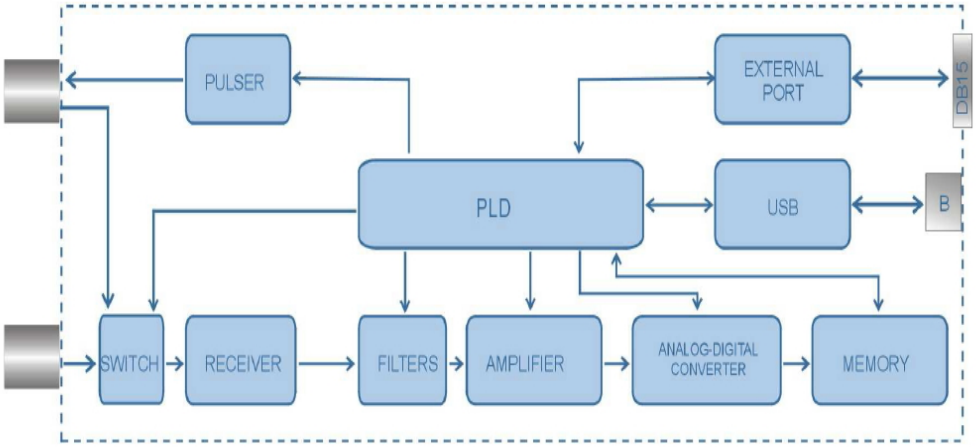

Figure 3.9: Block diagram of OPBOX(from OPBOX guide manual) [12]

Table 3.1: OPBOX features(from OPBOX guide manual)

Full Bandwidth	0.2 MHz $\sim$ 25 MHz
Input Impedance	50O hm, 10 pF
Adjustable Amplifier Gain Value	0 dB $\sim$ 68 dB
Additional Input Amplifier	24 dB
Sampling Frequency	100 MHz(Max)
Data Buffer	512 k Samples
Low Voltage	0 V
High Voltage	360 V
Charging Time	0 $\sim$ 3.1 us
Pulse Fall Time	20 ns

3.3.2 Time Gain Compensation (TGC) Gain

To reduce the power of the earlier and relatively strong noise reflected by air bubbles, and to amplify the later bottom surface reflection, TGC to increase the receiver gain over time is applied in the equipment setting. By observing sufficient experimental results, an appropriate TGC curve displayed by Fig.3.10 is obtained. This figure displays gain in decibels(dB), which is a common logarithmic unit used in acoustic tests to provide a relative measure of transducer voltage. Fig.3.11 shows the normal form of this curve. In these two figures, the total sampling time range is set to 0.35 ms in which the acoustic can propagate 1.26 m with 3600 m/s as the acoustic speed. This is sufficient to meet the project objective, which is to measure first year sea ice of less than 50 cm in depth.

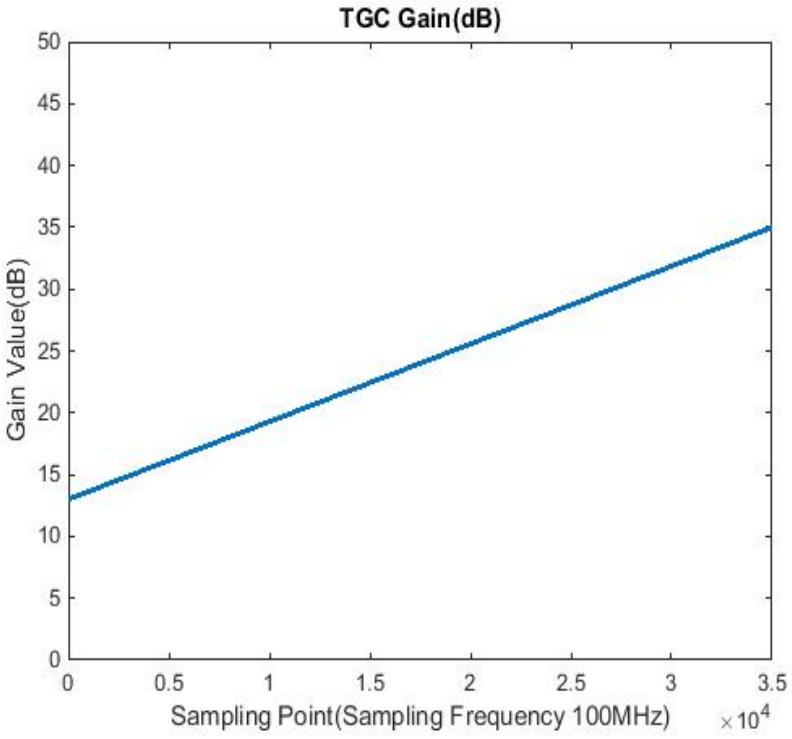

Figure 3.10: Decibel plot of TGC gain against time

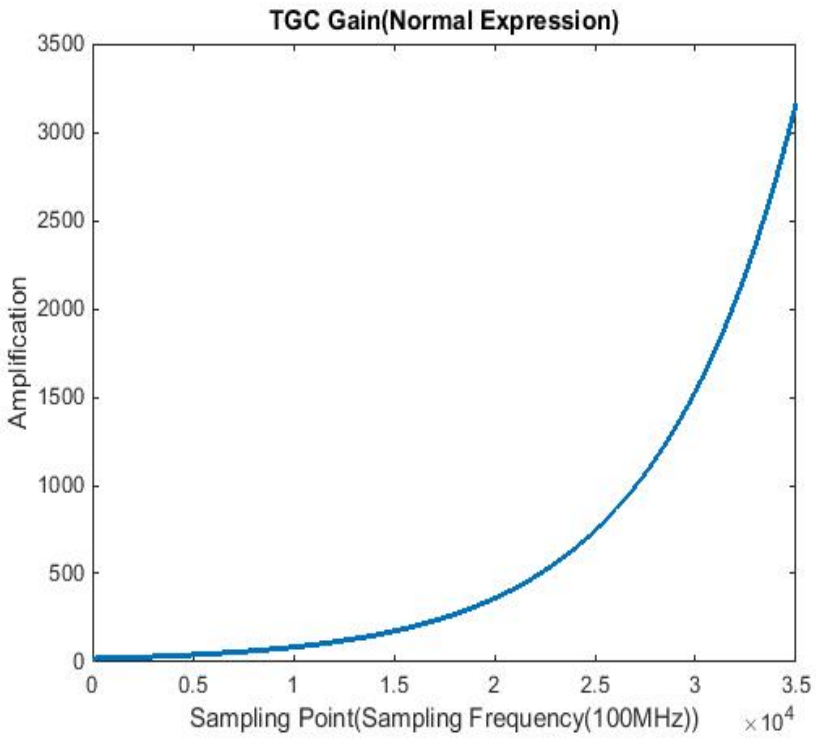

Figure 3.11: Normal plot of TGC gain against time

While using programming to control the OPBOX, the specific TGC gain values are written into a corresponding control register named DAC by calling the instruction **op−wrp−DoDAC** before starting sampling. The relationship between the value set in this instruction and its equivalent decibel value is displayed in Eq.3.3. From this equation, it can be seen that when gain is set up to $13dB$ then DAC value is 90, and when gain is set up to $35dB$ then DAC value is equal to 134 .

$$DAC = 2 * (GAIN[dB] + 32) \tag{3.3}$$

Therefore, the TGC curve shown in Fig.3.10 becomes the one shown in Fig.3.12 by changing the y-axis from decibel value to regular DAC value, and Eq.3.4 is its mathematical expression over the time change where x is sampling point.

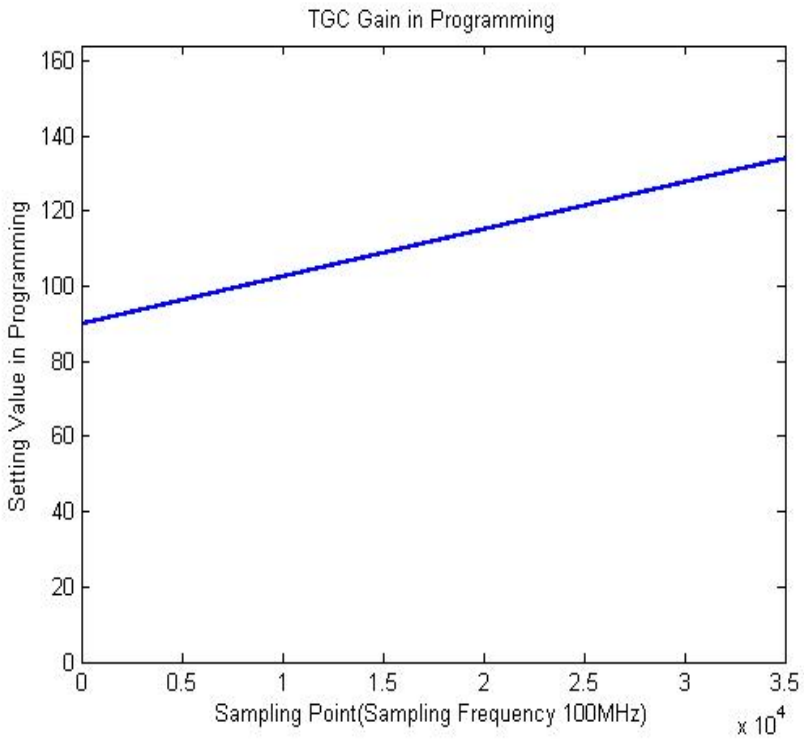

Figure 3.12: TGC gain in programming

$$y = \frac{44}{35000}x + 90 \tag{3.4}$$

The following two figures are the results of a 38 cm sea ice sample using different amplifier gain settings: 27 dB constant gain and proper TGC gain. While using constant gain, there are some sample values located before sampling point 7500 on the x-axis that overflowed. The bottom reflection that was expected to appear between the 20000 $\sim$ 25000 sampling point on x-axis is too weak that it might to be overlooked in later data processing. But this situation is effectively improved by using TGC gain as shown in Fig.3.13b.

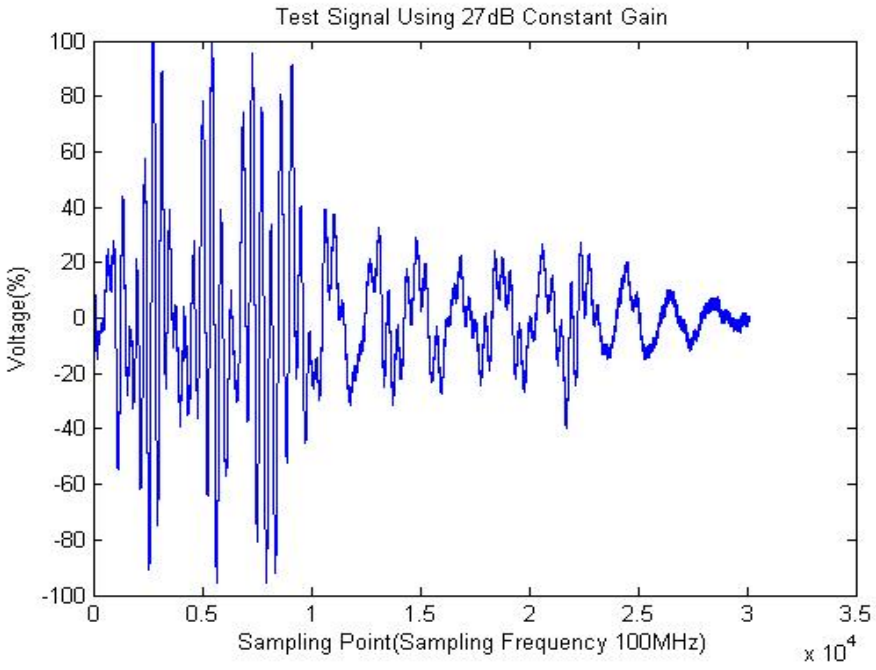

(a) Test result with constant gain

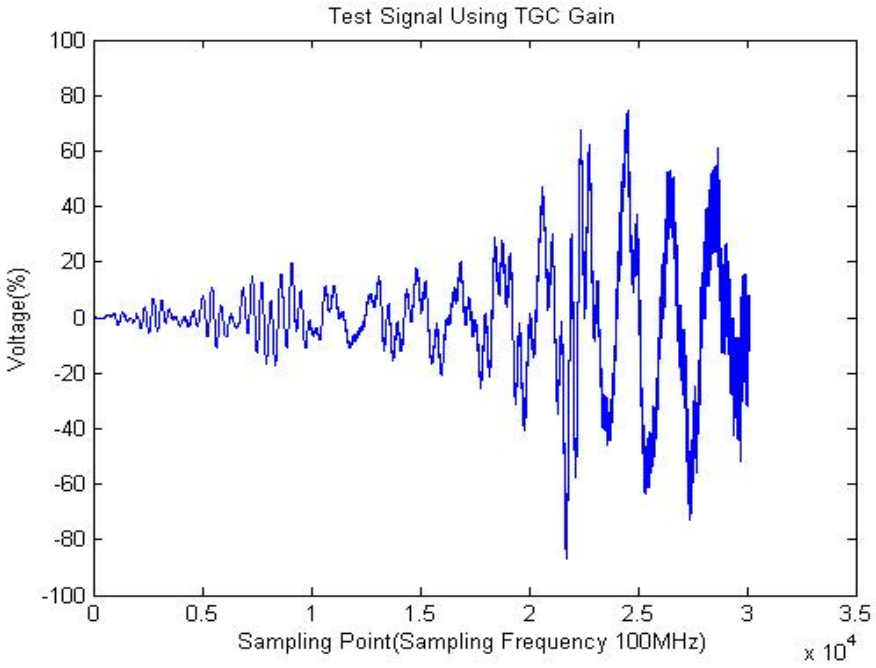

(b) Test result with TGC gain

Figure 3.13: Test results of using different gain settings

3.4 Channel Selector

3.4.1 Electronic Components

A channel selector, which is used to control the working sequence of the set of transducers is implemented by several electrical components including an mbed NXP LPC1768 microcontroller, OMRON G5V-2 relay, PN 2222A transistor and resister. They are deployed as indicated in Fig.3.16.

mbed LPC1768

The mbed NXP LPC1768 microcontroller as shown in Fig.3.14, designed for prototyping all sorts of devices, is a high performance Advanced RISC Machine (ARM) development board. The main processing unit of it is implemented by the ARM Cortex-M3, and its highest processing speed can reach 96 MHZ. As shown in Fig.3.14, it provides different peripheral interfaces with specific pins that may be required in further development, such as built-in Ethernet, USB Host and Device, CAN, ADC, DAC and other I/O ports. Its online compiler using C/C++ gives the developer a simple and convenient development environment. Some necessary libraries and frequently-used functions are supplied in its online tool as well. Once online compilation is done successfully, then downloading code into the mbed microprocessor will allow it to work independently. The mbed board can be powered by either a 5 V USB port or $4.5 - 9$ V power supply, and it can output two voltages through different pins: 5 V and 3.3 V logic voltages.

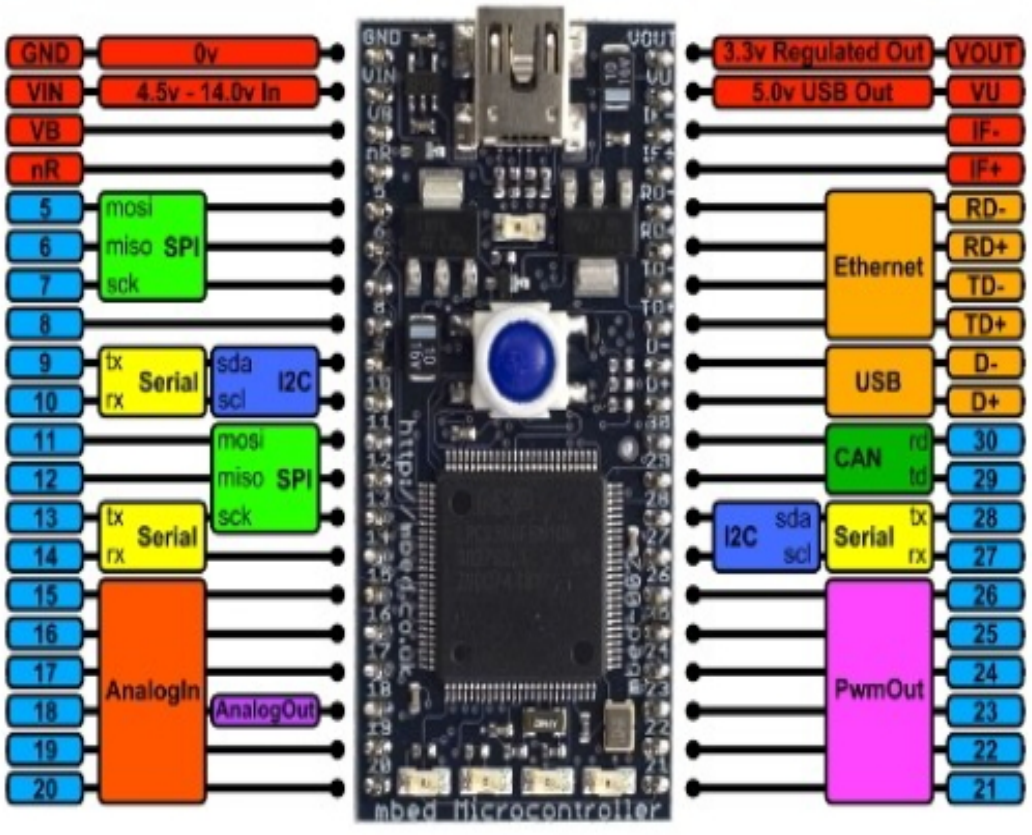

Figure 3.14: The mbed LPC1768 microcontroller(from mbed.org)[13]

OMRON G5V-2 Relay

A relay based on electromagnetism is mainly used to control a higher voltage circuit with a lower voltage. In this project, an OMRON G5V-2 relay using one coil to control two switches at the same time is applied in the channel selector circuit. Its appearance is shown on the left of Fig.3.15, and its internal structure is displayed on the right side. When the relay is inactive, or in other words when there is no current travelling through the coil, then the NC (Normally-Close) pin is connected, and the circuit is open. Conversely, if the relay is active, then the common pin is connected to NO (Normally-Open), and the circuit is close.

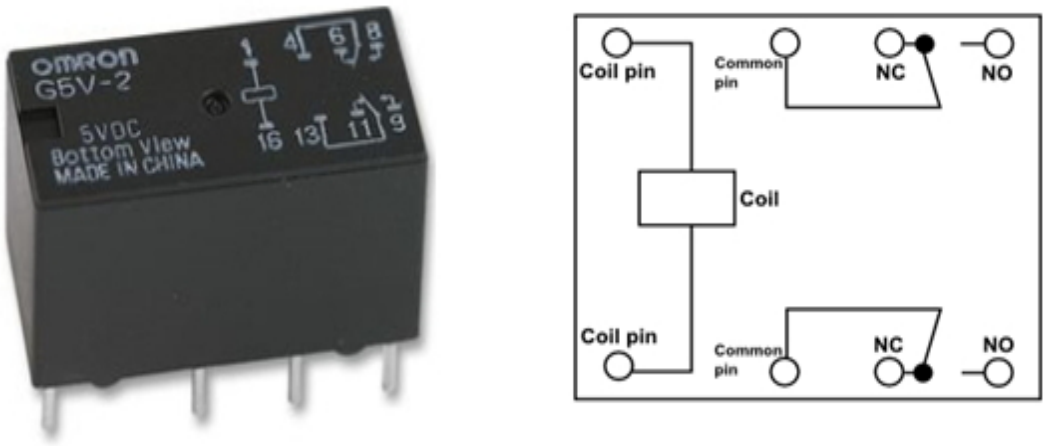

Figure 3.15: Relay OMRON G5V-2[14]

3.4.2 Channel Selector Circuit Design

In this project each transducer is required to work as an emitter and receiver at different times. Transducer is connected to the PE port and TT port of OPBOX through two relays controlled by mbed as shown in Fig.3.16. Programming mbed to give high logic voltage to the base pin of the PNP transistor located in front of the relay will allow higher current to go through emitter and collector successfully, so that the relay is activated. Therefore, the two relevant switches controlled by this relay are latched, and their connected transducers are selected to connect with the OPBOX ports PE or TT. All transducers are connected to OPBOX in this pattern, but at each time, there are only two output pins set up to high logic voltage, and the others are set to low; that is to say, there are two transducers working at that time: one connected to the OPBOX PE port is responsible for emitting the signal, and another one connected to the OPBOX TT port in charge of receiving the return signal.

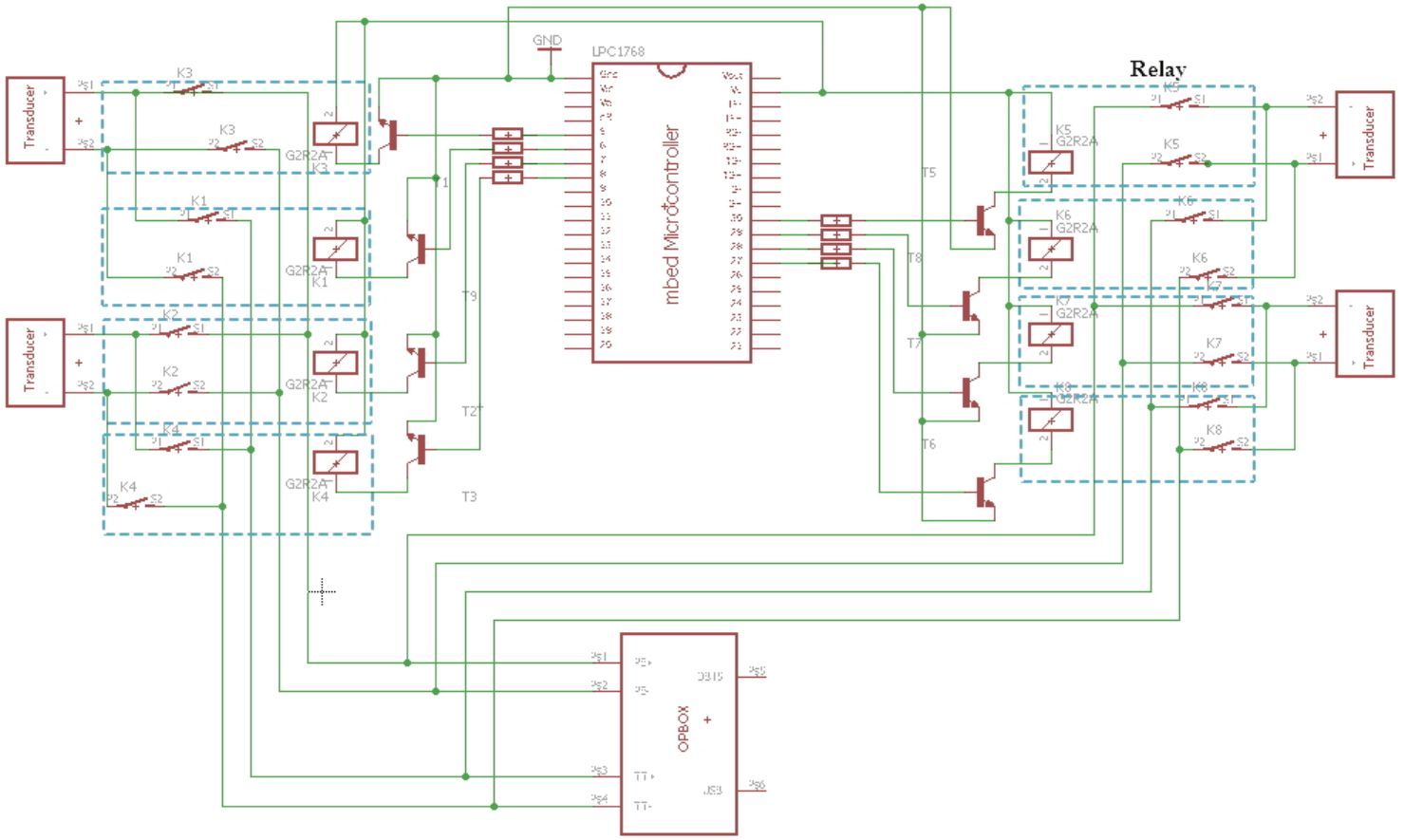

Figure 3.16: Schematic of channel selector

3.5 Laboratory Made Sea Ice

3.5.1 Laboratory Made Sea Ice Formation

Due to the limitations of the experimental conditions, in the early stage of the development, all tests mentioned in the later section are completed on laboratory made sea ice. The forming process of this kind of sea ice imitates the one in natural environment. These ice samples are made in a reefer belonging to the Memorial University thermal lab by freezing Atlantic Ocean seawater collected from Portugal Cove, near St. John's, Newfoundland, Canada. The reefer is a standard ISO 20 FT shipping container located outdoor and insulated with a refrigeration unit. Its outside and inside appearances are shown in Fig.3.17. Although its lowest temperature can be adjusted to $-30°C$, high electrical consumption can cause the power to shut down occasionally. To ensure the reefer can work well during the whole sea ice forming process, its inside temperature is maintained at $-15°C$.

Figure 3.17: Outside and inside view of reefer

As described in Section 2.2.1, compared with fresh water ice, the forming process of sea ice is more complicated. Before freezing up, it has to first expel its dissolved salt. In a natural environment, there is only vertical heat exchange. To mimic as closely as possible the formation of real sea ice, a special mould was constructed as shown in Fig.3.18. It is a 39"$(L)*19$"$(W)*13(H)$" plastic tote wrapped around by 2" pink rigid foaming to pad minimize lateral heat transfer, leaving only two smaller sides exposed to air to achieve one directional heat flux and thus mimic the formation process of real sea ice. Therefore, seawater will freeze up from two sides towards the middle, where most of the expelled salt is centred.

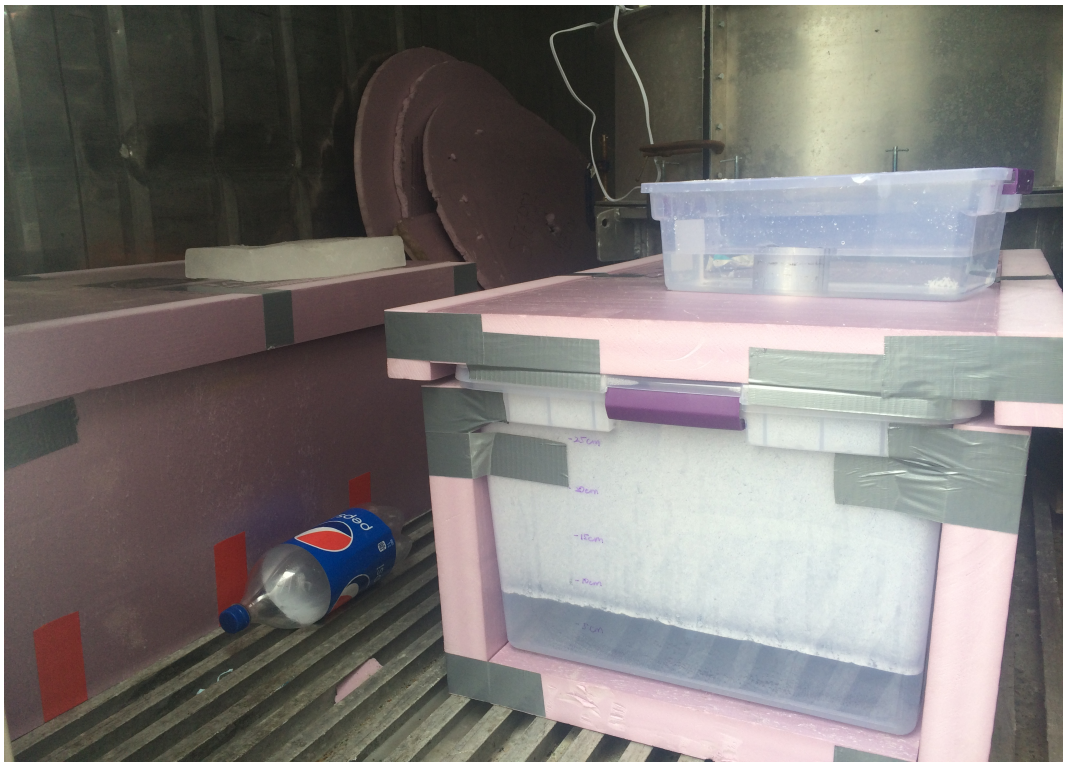

Figure 3.18: Special mould for sea ice making

3.5.2 Laboratory Made Sea Ice Features

Due to the high salinity of the middle, it can not become solid and is unusable for experiments in this project. Fig.3.19 and Fig.3.20 display a laboratory sea ice sample made by this special mould. From Fig.3.19, an overview of a sea ice sample, it can be seen that the area near the two sides are solid and they are usable for experiment in this project, but the middle part is slushy and contains a lot of cracks that may not happen in a natural environment. From Fig.3.20, which is a detailed picture of Fig.3.19, it can be observed that laboratory made sea ice does contain a fair number of air bubbles and some longitudinal brine pockets indicated by red arrow. Both of these are important features of natural sea ice.

Figure 3.19: Laboratory made sea ice

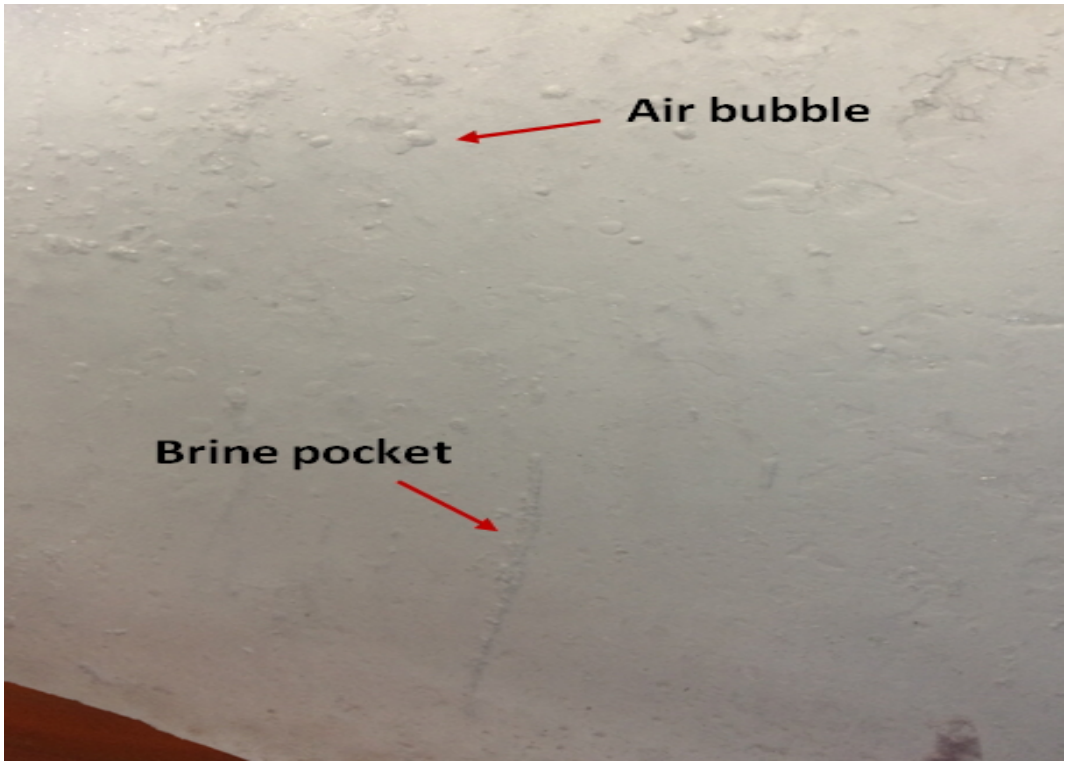

Figure 3.20: Detailed picture of laboratory made sea ice

3.5.3 Speed of Sound in Laboratory Made Sea Ice

The speed of sound in sea ice varies based on its salinity, temperature and impurity. To measure the correct thickness, the appropriate speed of sound in laboratory made ice is the first issue that needs to be addressed. Therefore, the traditional TT mode that puts two identified transducers on both sides of a 7.8 cm sea ice sample is used to collect direct reflections. Fig.3.21 shows the result of the receiver placed on the bottom of sea ice to detect the signal over 2177 sampling points, which equals 21.77 µs at a 100 MHz sampling frequency. With a known thickness of 7.8 cm, the sound speed 3580 m/s for laboratory made sea ice can be estimated.

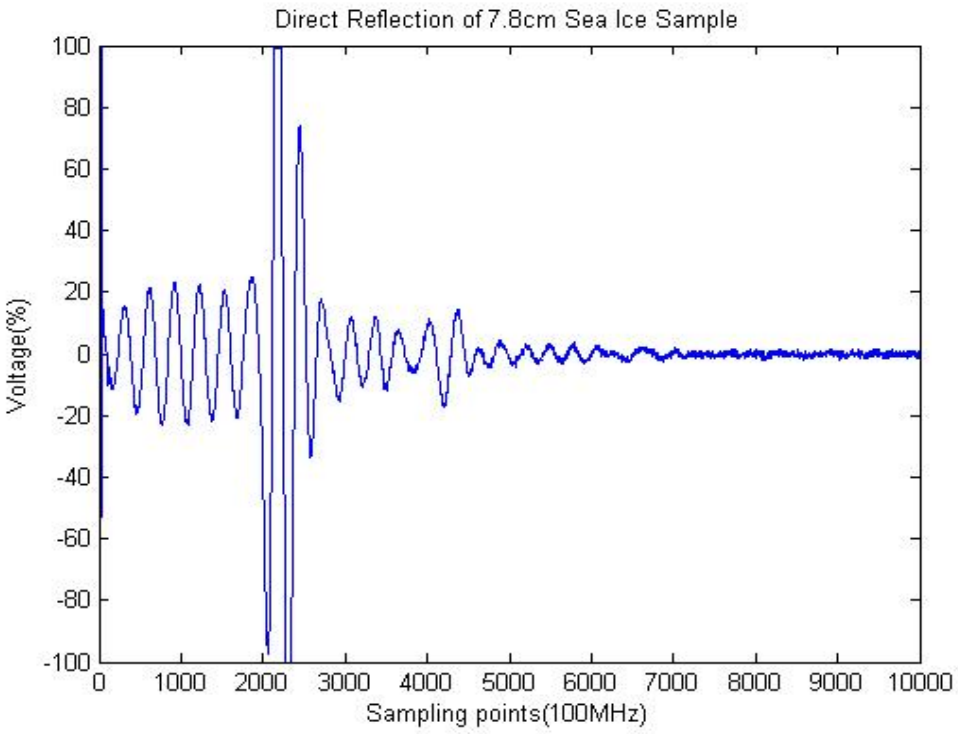

Figure 3.21: Direct reflection of 7.8 cm sea ice sample

3.6 Couplant

In making ultrasonic acoustic measurements on a surface using transducers, the contact between the transducer and the surface must be such that there is efficient transmission between the transducer and the surface material. Because air is a high attenuation medium for acoustics, acoustic transducers are very inefficient in air. Therefore, it is necessary to use an acoustic coupling medium in order to efficiently transmit the energy from the sensor to the test material. Couplant materials that are often used include ultrasonic gel, O-ring grease and Vaseline™[23]. In this project, the couplant cannot be water soluble, so ultrasonic gel is not suitable for sea ice tests. Another aspect that needed to be considered is the low freezing point. In future applications, the sensor system developed in this thesis is intended to work in harsh, cold environ-

ments where the lowest temperature can be −50°C. This limiting condition reduces the range of couplant choices. O-ring grease, Vaseline and kerosene all have lower freezing point than −50°C. Vaseline is a thick gel in normal circumstances, but with the decrease in temperature it become more and more solider and is very difficult to apply on either a transducer or the sea ice surface. For this reason, Kerosene and O-ring grease are both better than Vaseline. Kerosene is a liquid and O-ring grease is a very soft cream. In addition, the author also tried another method of freezing transducer into sea ice a little bit without using any couplant. Fig.3.22 shows the comparison of using different couplants and methods. From this figure, it can be seen that keronsene and O-ring grease provides a similar transmission efficiency, and both provide higher efficiency than freezing the transducer into an ice sample. Finally, out of consideration of safety issues the author selected O-ring grease as the best couplant in this project.

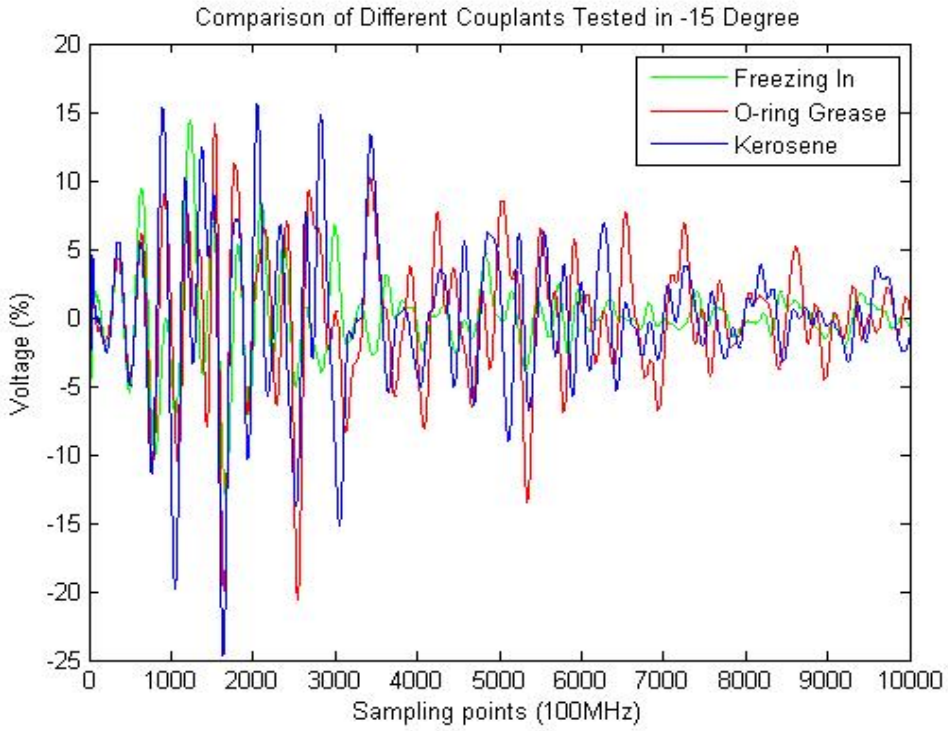

Figure 3.22: Comparison of different couplants

3.7 Experimental Procedure

The experimental procedure used is as following:

1. Prepare a same size plastic tote as mentioned in previous section, and place four 5 cm height aluminium spacers at each corner to support the sea ice sample.

2. Pour seawater into a plastic tote, then put four 5 cm high aluminium spacers at each corner to support the sea ice sample.

3. Place the sea ice sample on a spacer horizontally, and ensure that its bottom surface has been soaked into the water.

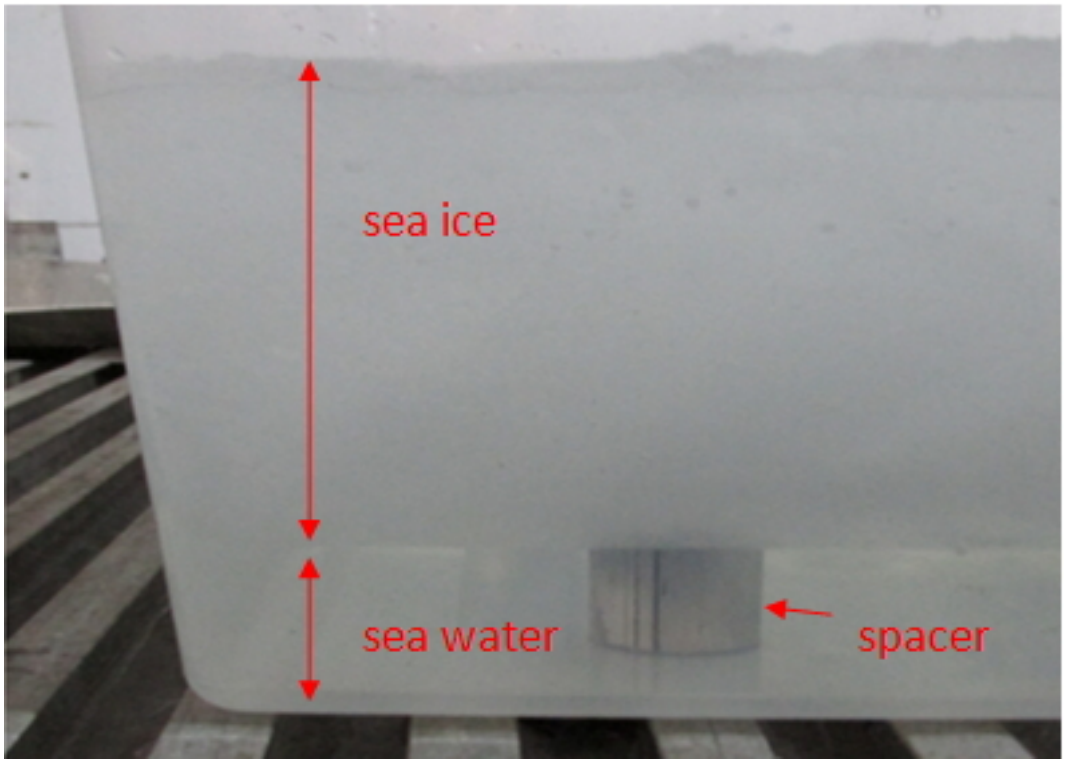

Figure 3.23: Experiment preparation

4. Use a warm aluminium flat plate to smooth the sea ice surface.

5. Place a plastic pattern containing ten holes marked with a red number on the sea ice top surface to imitate the use of ten transducers.

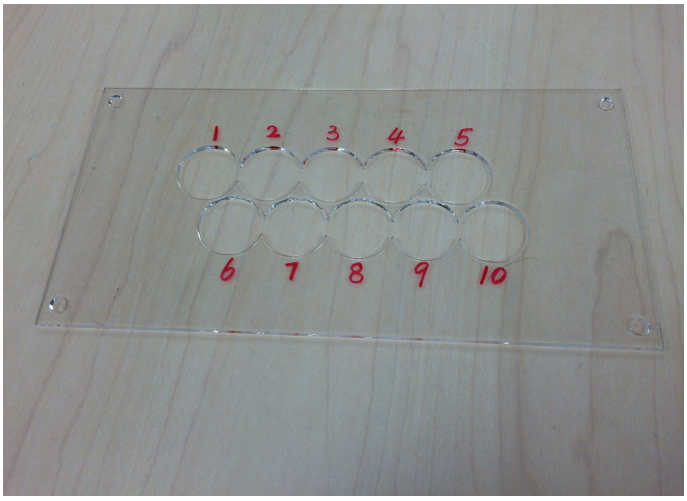

Figure 3.24: Plastic pattern

6. Place two transducers in two adjacent holes and collect data, then change to another adjacent two holes to do the next test. There are 34 different combinations with just ten holes. All these combinations are displayed in Table 3.2. Exchanging the positions of emitter and receiver, the acoustic signal propagation path will be reversed, and the positions of impurity reflections will change.

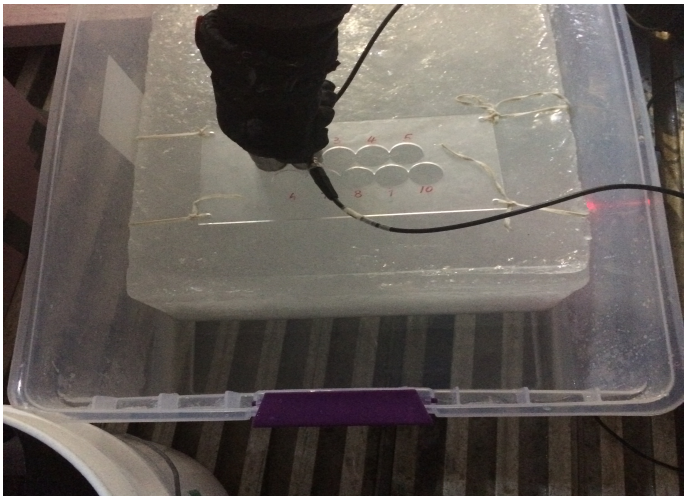

Figure 3.25: Collecting data

7. Analysis collected data as described in Chapter 4.

Table 3.2: Combination of imitating ten transducers

	Emitter Position	Receiver Position		Emitter Position	Receiver Position
1	1	2	18	6	1
2	1	6	19	6	2
3	2	1	20	6	7
4	2	3	21	7	2
5	2	6	22	7	3
6	2	7	23	7	6
7	3	2	24	7	8
8	3	4	25	8	3
9	3	7	26	8	4
10	3	8	27	8	7
11	4	3	28	8	9
12	4	5	29	9	4
13	4	8	30	9	5
14	4	9	31	9	8
15	5	4	32	9	10
16	5	9	33	10	9
17	5	10	34	10	5

Chapter 4

Data Processing

4.1 Signal Filtering

To avoid missing any potential information, the built-in analog filter of OPBOX is turned off while collecting raw data from different positions. But a 4th order Butterworth bandpass filter designed by Matlab is applied later as the first step of data processing to reduce background noise. Fig.4.1 displays the frequency response of this filter. The x-axis of this figure is frequency, and the y-axis is the attenuation index expressed in dB. From this figure it can be observed that the passband of this filter is very flat, and the stopband sharply decreases. As is well known, when the order of the filter increases, the filter will be much closer to the ideal one, but it also will cause greater delay in the time domain. Considering these issues, 4th order is selected as the appropriate one. The central frequency of the piezoelectric transducer used in all experiments is 250 kHz. Due to the frequency shift phenomenon mentioned in the later paragraph, the passband of this filter is set up to be 150 kHz $\sim$ 350 kHz. Any frequency component beyond the desired frequency range will be attenuated sharply, especially the ones lower than 150 kHz. Fig.4.2 displays a raw signal obtained from a

16 cm sea ice sample. Comparing this figure with Fig.4.3, it can be observed that the signal becomes smoother after processing by the Butterworth filter. Most background noise is filtered out in this step.

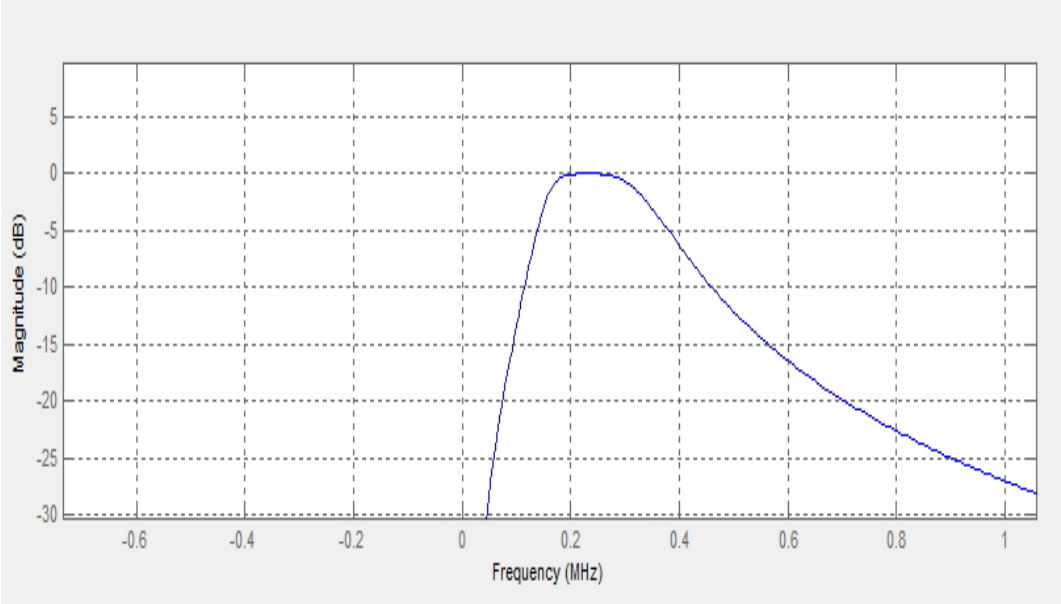

Figure 4.1: Frequency response of 4th order butterworth filter

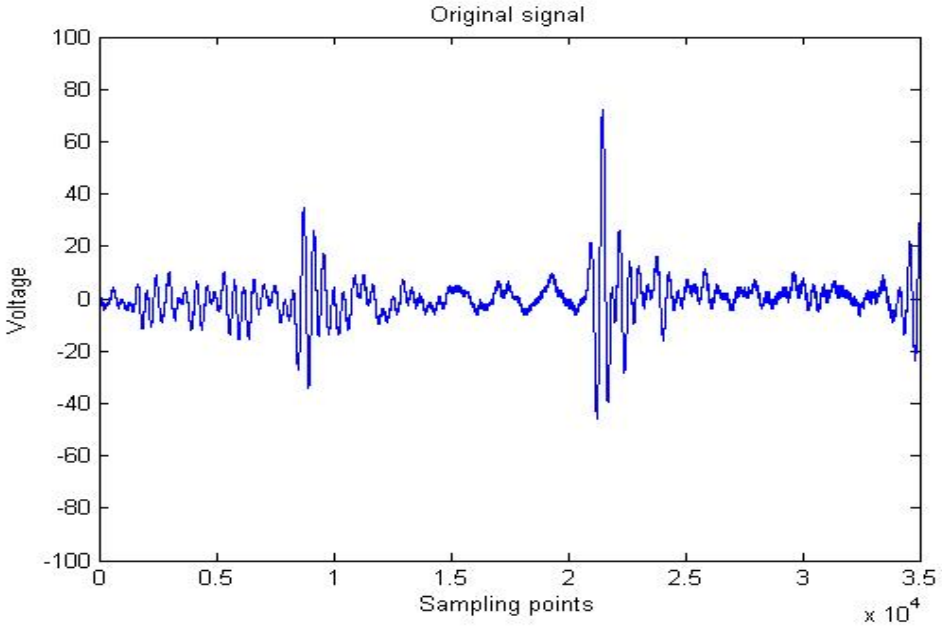

Figure 4.2: Raw signal

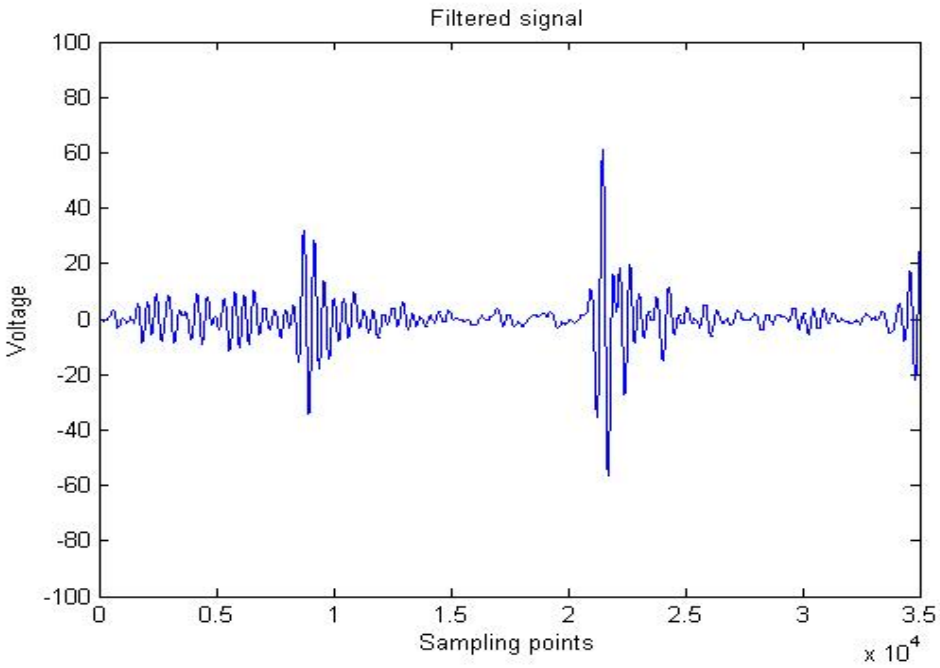

Figure 4.3: Filtered signal

4.2 Short Time Fourier Transform

The Fourier Transform (FT) is a significant technique in Digital Signal Processing (DSP) used to transform the signal from the time domain to the frequency domain. By using this method, any random signal can be decomposed to a set of sinusoidal signals each with a different frequency, phase and magnitude as shown in Fig.4.4. The Discrete Fourier Transform (DFT) is a form of the discrete-time FT used to process digital signals represented by limited sampling points in both time and frequency. Eq.4.1 is the mathematical expression of the DFT where the finite length signal is represented by $x[n]$, and its corresponding DFT is denoted by $X[k]$.

$$X[k] = \sum_{n=0}^{N-1} x(n) e^{-j\frac{2\pi kn}{N}}, \qquad k = 0, 1..., N-1 \tag{4.1}$$

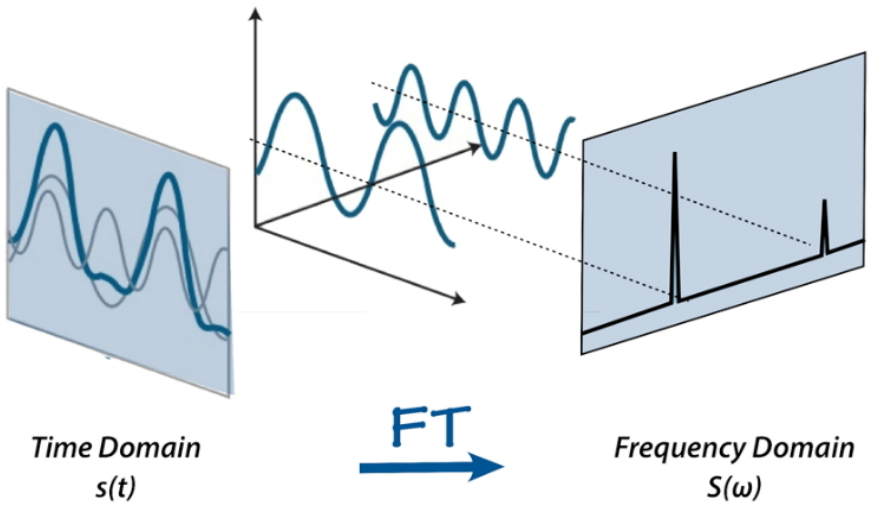

Figure 4.4: Fourier Transform [15]

The Short Time Fourier Transform (STFT), which is an extended format of the FT, can model sinusoidal frequency distributions over local signal segments and track their changes over time. This is done by windowing a large signal into small overlapped segments and then applying the DFT to each piece. This process is expressed well by Fig.4.5. In this figure, it can be observed that a window function $w(n)$ whose length is N shifts from the right to left, with overlapping, thus dividing the complete signal into many segments. The m-th windowed segment is given by Eq.4.2. Then taking the DFT of each windowed segment as shown in Eq.4.3, the frequency distribution of the whole signal over time can be obtained.

$$s(m,n) = x[n] \cdot w[n - m \cdot N/2] \tag{4.2}$$

$$S(m,k) = DFT\left\{x(n) \cdot w(n - m \cdot N/2)\right\} \tag{4.3}$$

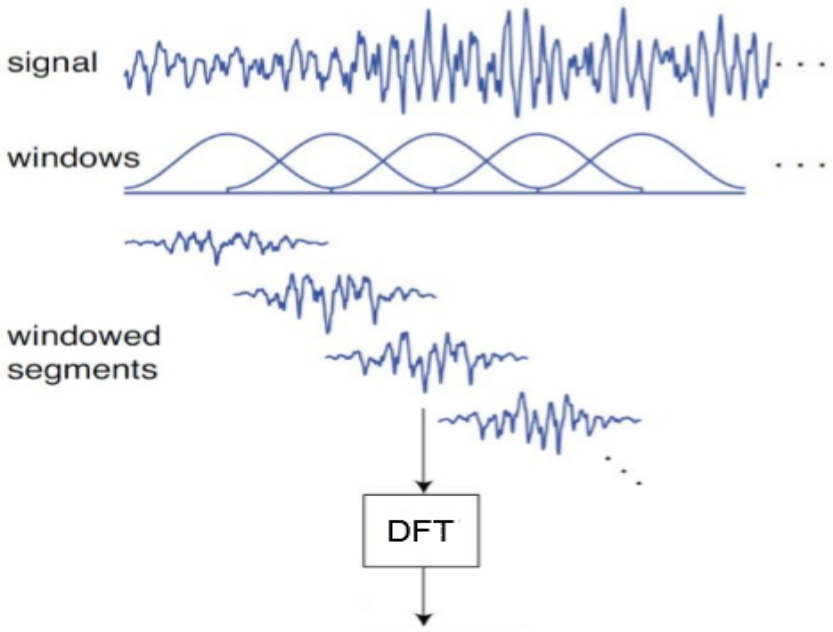

Figure 4.5: Short time fourier transform process [16]

By using the STFT to track the frequency change of the signal it can be observed when a 250kHz acoustic pulse occurs. After applying the STFT to the above filtered signal shown in Fig.4.3, its 3D frequency spectrum is obtained and displayed in Fig.4.6 whose x-axis represents time; y-axis represents frequency, and z-axis demonstrates power distribution over different frequencies and over time. According to previous research [24], the central frequency will experience a down shift when an acoustic wave propagates in a porous medium which will lead to high scattering attenuation. The cause of this shift is that higher frequency components are always more attenuated than those of a lower frequency. In this case, due to the existence of air bubbles, sea ice can be considered as a kind of porous medium; thus a down shift of the acoustic central frequency may occur during the measurement value to some extent. Also, regarding the spectrum leakage property of the DFT caused by finite-length sampling, the power of acoustic pulse which is supposed to be located at the 250

kHz in frequency damain is spread out to its nearby frequencies. Through observing some test results, the author set this frequency area to between 150 kHz and 350 kHz. As mentioned before, the STFT windows the whole signal into small segments over time. To make the position of reflection easier to be observed, author adds all Power Spectrum Density (PSD) values, which are in the same segment and in the range of 150 kHz and 350 kHz, to simplify the complicated frequency spectrum displayed in Fig.4.6 into a power curve as shown in Fig.4.7.

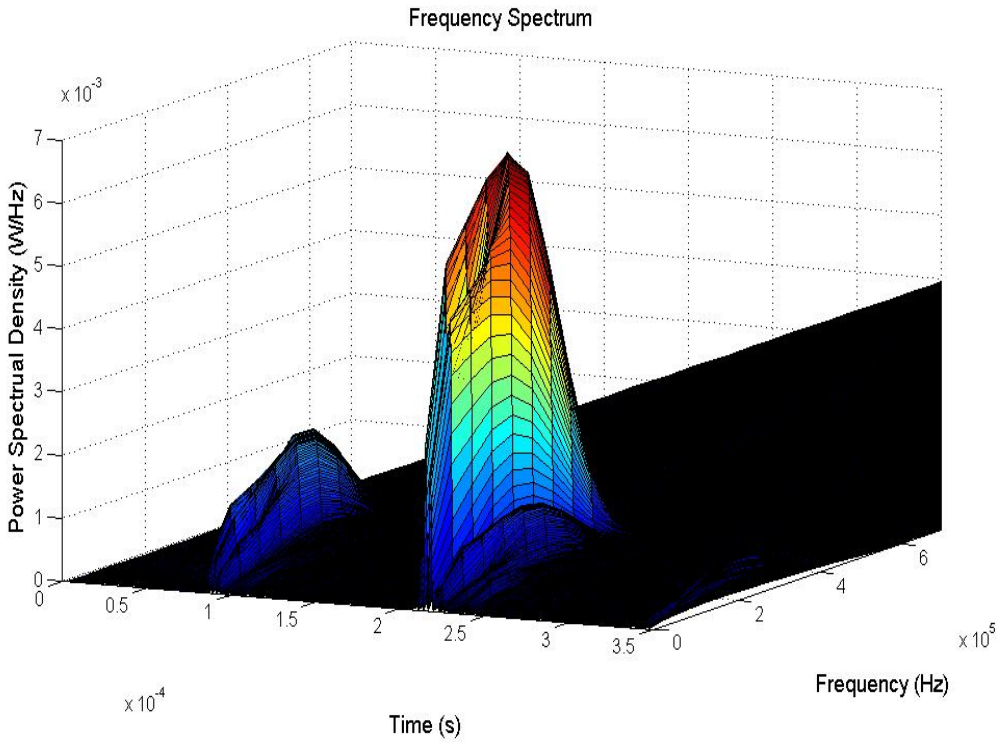

Figure 4.6: STFT Frequency spectrum

4.3 Selection of Valid Reflections

Fig.4.7 displayed the power curve of Fig.4.6. In this figure, it can be seen that there are more than one reflection peaks. By setting an appropriate peak threshold, minimum peaks' gap and peak sharpness, only a few of them marked with a red spot are

selected as valid reflections. Their x-coordinates represent the times when these valid reflections appear. Unfortunately, it is impossible to identify from where they are reflected back, whether from the impurities within the sea ice or from the bottom surface. In other words, it is hard to find the desired reflection from the bottom surface by a single test.

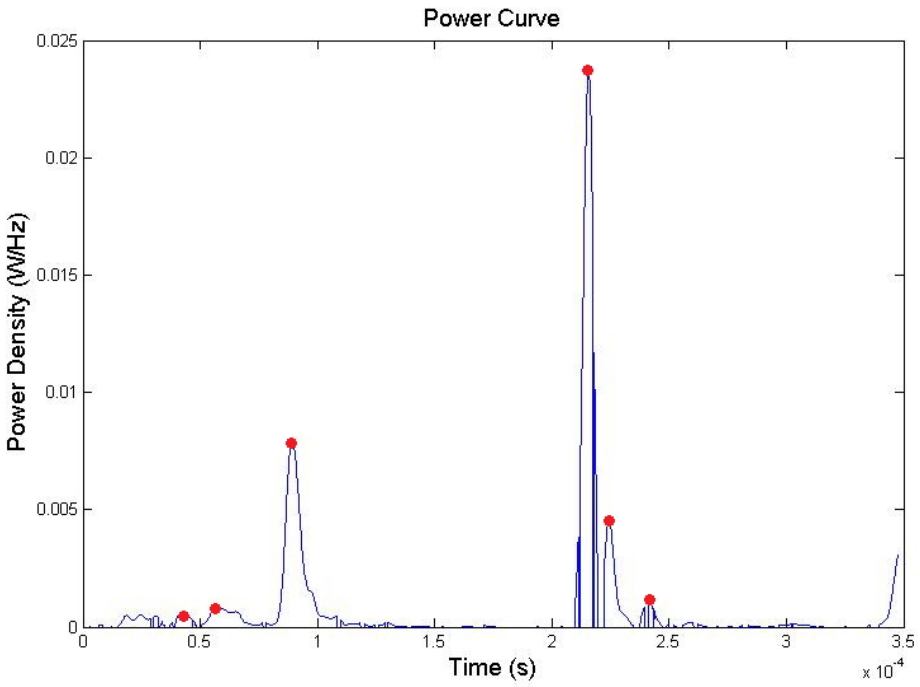

Figure 4.7: Power curve of 16.2 cm sea ice

4.4 Extraction of Final Result

Based on the random distribution of impurities and fixed position of the bottom surface, the desired result can be extracted by observing 34 signals collected from multi-locations as shown in Fig.5.6. To obtain this figure, the following steps are performed. At first, the valid reflections of each signal are found by using the above data processing methods. Second, all reflections are gathered from different signals

and put into one matrix to represent this information more clearly. Table 4.1 displays a small part of this matrix. A ‘1’ in the table indicates the actual peak and ‘0’ indicates a non-peak. The time from 2.4 µs prior to 2.4 µs after the time stamp at which the reflection appears are included and valued as ’1’ due to the time resolution of the STFT. Fig.5.6 is another expression of the whole matrix by adding all values in the same column (same segment over time) together. This figure displays how many reflections occur at each time stamp, with 34 signals overall. The moment containing the highest number of reflections is considered the best estimated time that the sea ice-water surface reflection is received by the sensor.

Table 4.1: Peak record

Time Stamp(us) / Signal Number	20.56	20.68	20.80	20.92	21.04	21.16	21.28	21.40	21.52	21.64	21.76	21.88
1	0	0	0	0	0	0	0	0	0	0	0	0
2	0	0	0	0	0	0	0	0	0	0	0	0
3	1	1	1	1	1	1	1	1	1	1	1	1
4	1	1	1	1	1	1	1	1	0	0	0	0
5	1	1	1	1	1	1	1	0	0	0	0	0
6	0	0	0	0	0	0	0	0	0	0	0	0
7	0	0	0	0	0	0	0	0	0	0	0	0
8	1	1	1	1	1	1	1	0	0	0	0	0

Chapter 5

Results and Discussion

5.1 Comparison of Different Frequency Transducers

Compared with the 500 kHz transducer, the 250 kHz is more suitable for this experiment. Fig.5.1 displays two power curves obtained from tests which are performed on the same sea ice sample of 12 cm depth, with the same location but a different transducer frequency. The blue power curve is the one using the 250 kHz transducer, and the other one is using 500 kHz. The reflections marked with a red spot are come from the bottom surface of ice sample. From this figure, it can be observed that the signal from the 250 kHz transducer has less interference from impurities and provides a stronger reflection than 500 kHz transducer. This is because the wavelength of 250 kHz is two times that of 500 kHz. Only an impurity whose diameter is larger than half of the wavelength may block the propagation path and consume the acoustic energy. For the same propagation path, the signal from the 250 kHz transducer can skip larger bubbles and save more power than that from the 500 kHz. This experiment is finished on 12 cm sea ice. As is well known, the acoustic power consumption will

increases as the thickness of the sea ice increases. In contrast, its reflection power will decrease. On account of the poor reflection power of the 500 kHz transducer that may not be detected in measuring thicker ice samples, a 250 kHz transducer is selected as the appropriate one applied in later experiments.

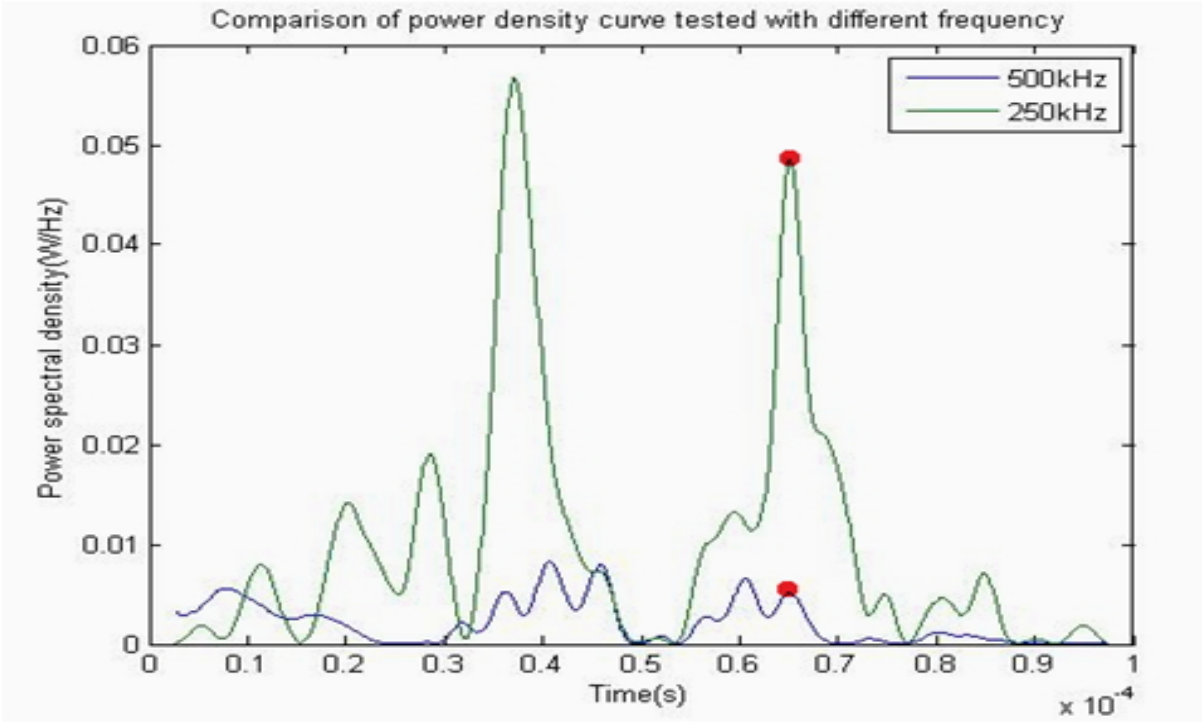

Figure 5.1: Power curve comparison of 250 kHz and 500 kHz transducers

5.2 Confirmation of the Presence of Sea Ice/Seawater Reflection

Before measuring the thickness of the sea ice sample, another pre-test is performed to confirm there is indeed a reflection coming from the bottom surface (sea ice/seawater interface). First, the ice sample and other equipment needs to be set up normally without pouring seawater into the plastic container. At that time, the bottom inter-

face of sea ice is sea ice/air. After collecting a signal called ice/air at a certain place, then sufficient cold seawater should be poured into the container until the bottom surface of the ice sample soaks into the seawater. Next, the second signal called ice/water should be collected without moving transducers or changing any other settings. While doing this test, it is observed that the power curve shown in Fig.5.2 changes from the blue one to the green one when seawater touches the bottom surface of the ice sample. Also, from this figure, an interesting phenomenon is found in that most reflections of these two curves roughly occur at the same position and same power level except for the two that are marked with red spots. Although these two occur at the same place, one is much stronger than the other one. This is because most reflections are reflected by the same inherent impurities, and these two are reflected by different reflectors: air and seawater. Otherwise, due to the large impedance mismatch between sea ice and air, the strongest reflection, which is also the one of red spots of the blue curve, should be the bottom surface reflection. Based on the above analyses, it can be said that the other one marked with the red spot on the green curve is reflection caused by the bottom interface sea ice/seawater. Therefore, it can be confirmed that sea ice/seawater reflection is detectable in the case.

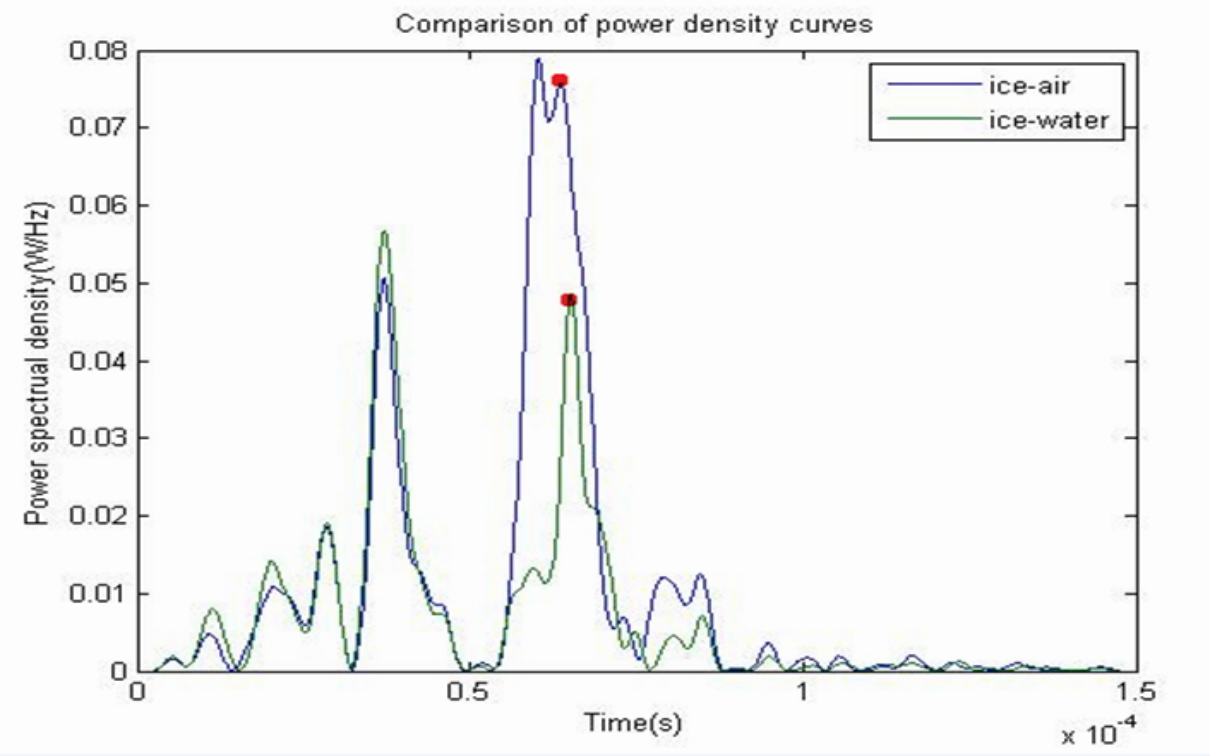

Figure 5.2: Power curve comparison of reflections coming from different interfaces

5.3 Comparison of Different Freezing Duration

Compared with the one-week-old laboratory made sea ice sample shown in Fig.2.3, the one-month-old sample made by the sample method but different freezing duration has a better quality. During longer freezing times, more air bubbles are expelled and inherent brine pockets join each other to form new, bigger ones or large drainage terminals. In other words, there are more clear propagation paths for acoustic. Fig.5.4 is the final test result of the one-week-old ice sample. Fig.5.5 shows the result of the same ice sample, after one-month of freezing with some additional thickness due to freezing longer. There are 8 more detectable bottom surface reflections in the latter case.

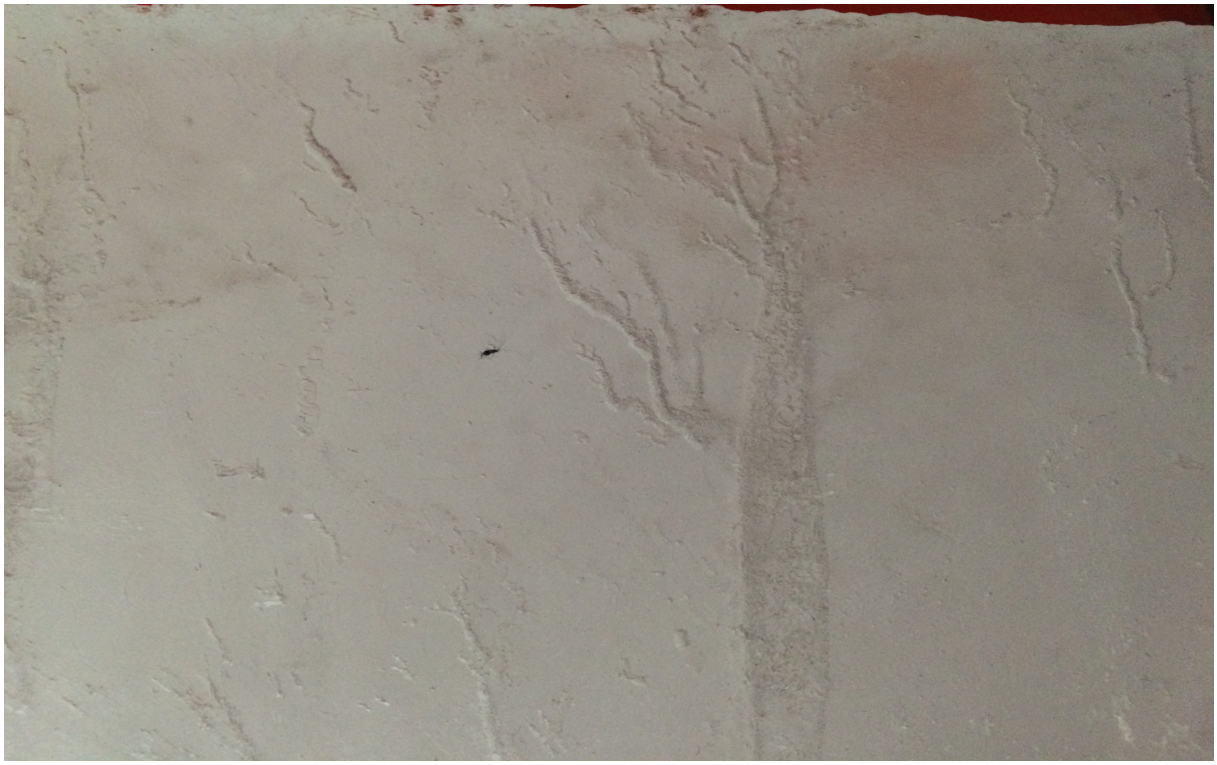

Figure 5.3: Details of the one-month-old sea ice sample

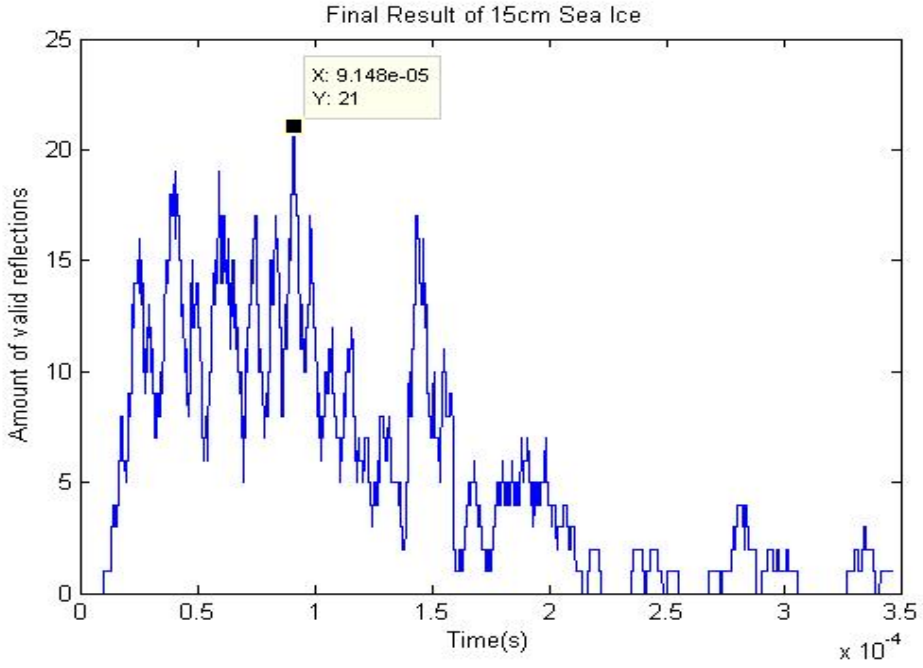

Figure 5.4: Result of 15.2 cm sea ice (one week of freezing)

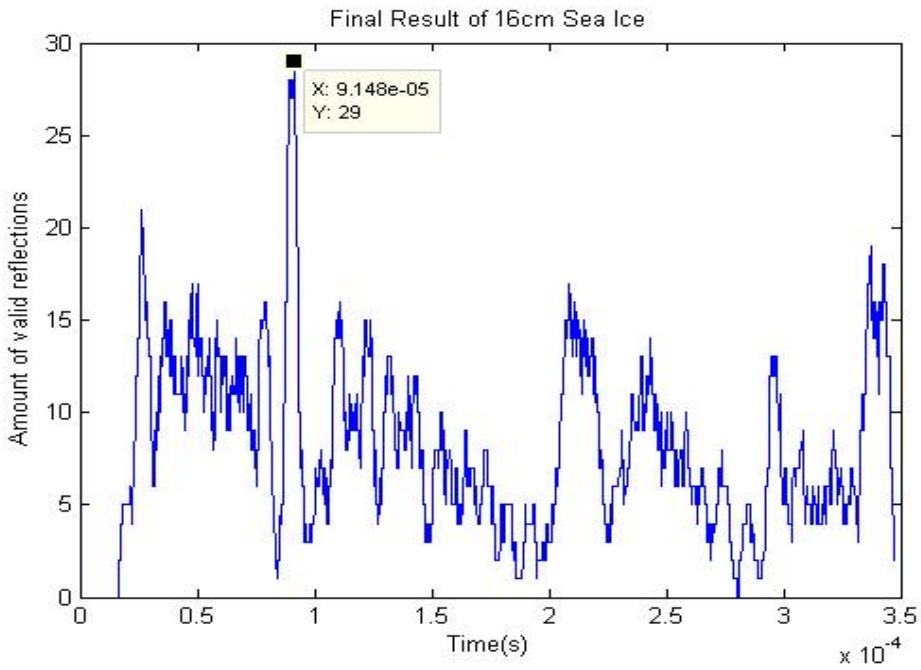

Figure 5.5: Result of 16.2 cm sea ice(one month of freezing)

5.4 Final Results of Different Thickness

Fig.5.6, Fig.5.7, Fig.5.4 and Fig.5.5 show the final results for lab made sea ice sample with thickness 4.3 cm, 12 cm, 15.2 cm and 16.2 cm. Their highest amounts of reflection occur at 27.4 µs, 73.2 µs,91.5 µs and 91.5 µs. In terms of thickness, these times are corresponding to 4.9 cm, 13.1 cm, 16.2 cm and 16.2 cm. Table 5.1 shows a comparison of actual thickness measured by using measuring tape and the tested thickness obtained by using this sensor system. All errors are below 5 cm what is the maximum tolerable error of project requirement. Therefore, these test results are acceptable. Errors come from two aspects. One is from the transducer. The higher frequency transducer has better resolution, but poorer penetration ability. In sea ice, air bubble size may be over 4 mm. Any object larger than a half transducer wavelength could block the transmission path to the lower surface. Due to this reason, we cannot

increase the transducer frequency to obtain a lower error rate. Another aspect is our data processing method which uses limited sampling points, with parameters chosen based on the current, limited, laboratory experimental results. It may be improved to reduce errors in the future after completing more experiments.

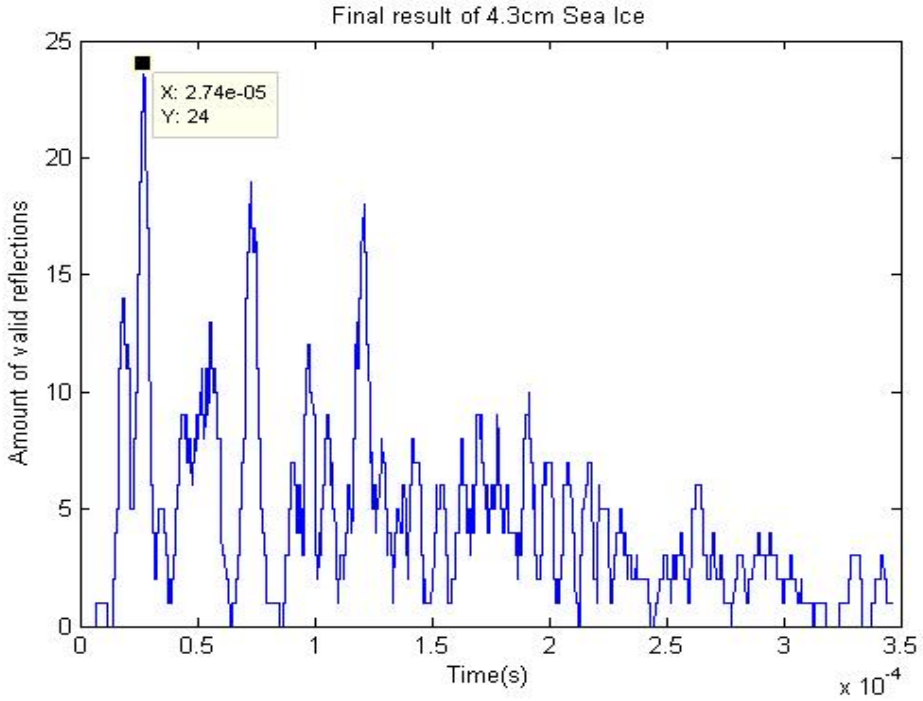

Figure 5.6: Result of 4.3 cm sea ice

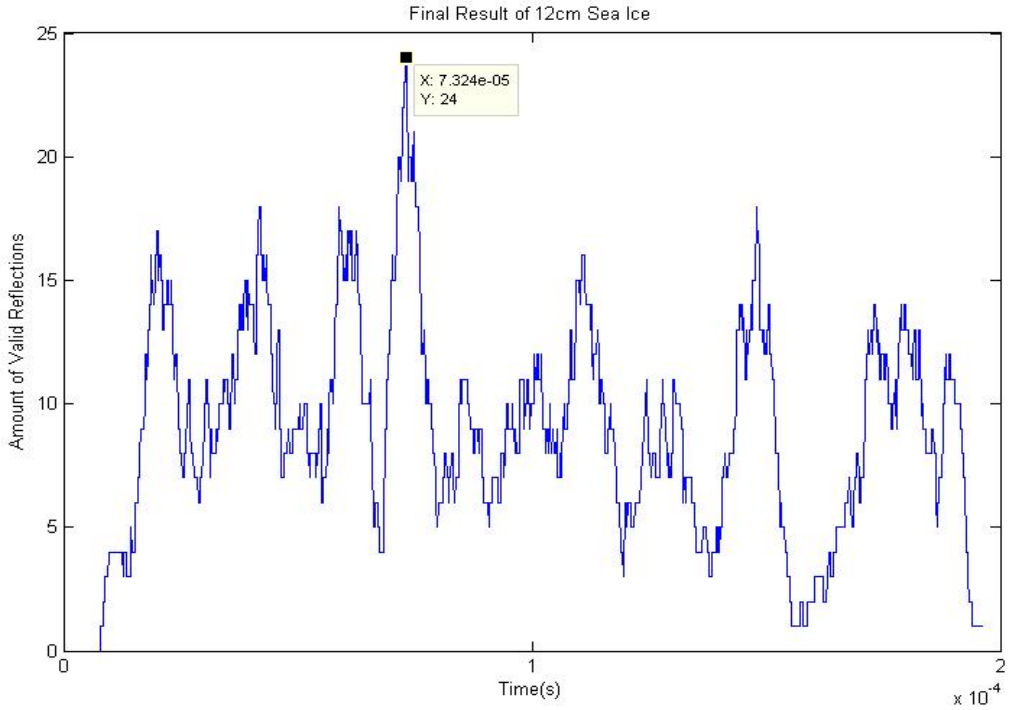

Figure 5.7: Result of 12 cm sea ice

Table 5.1: Comparison of real thickness and measured thickness

Actual Thickness by Tape Measure	Acoustic Measured Thickness	Error
4.3 cm	4.9 cm	0.6 cm (14%)
12 cm	13.1 cm	1.1 cm (9%)
15.2 cm	16.4 cm	1.2 cm (8%)
16.2 cm	16.4 cm	0.2 cm (1%)

5.5 Discussion

So far, this method has been applied on laboratory made sea ice samples successfully. The bottom surface of this kind of ice is flat. As mentioned in section 4.4, to extract

the final result, the time resolution of the STFT is important since the STFT segments the whole signal into small time periods, and any detected reflection is recognized as occurring at the middle of this time period. But in reality, this reflection might be appearing at any time in the period. Therefore, by changing the time to thickness, each reflection is not just a point but is expanded to an area (± 1 cm). For example, if a reflection occurring at 4 cm, then in this system the whole depth from 3 cm to 5 cm is recognized as from where the reflection comes. Therefore, the final result is actually a mean value of the thickness.

In a natural environment, normally, a first year ice floe, which is a kind of young ice, experiences less serious collisions with each other. Though its bottom surface is a little bit uneven, there may not be a lot of sharp humps caused by collision. In future field test, if the bottom surface is too rough and uneven, in order to get a reliable mean result, there are two things that have to be done to solve this problem: changing parameters of algorithm to enlarge the reflection area (± 2 cm or bigger); and doing more tests at different locations.

Chapter 6

Conclusion and Future Work

6.1 Conclusion

A prototype model of an acoustic sensor system used to measure the thickness of first year sea ice has been developed and tested in the Autonomous Ocean System laboratory of Memorial University. This autonomous system can be left on the ice surface for a while to collect data and then save this data into a hard drive regularly after the power is turned on. An algorithm developed in a Matlab environment is used in later data processing. Through using some significant Digital Signal Processing methods, it can analyse huge amount of data and extract reliable results. All functions of this sensor system work well in harsh, cold environments. In addition, several measurements on lab made sea ice samples have been successfully completed. Besides designing and implementing a sensor system, making good quality sea ice which should have similar features as natural ice is another significant part of this project. After numerous attempts, a special mould and process was developed. However due to the mould size limitation, the 50 cm requirement could not be reached.

6.2 Future Work

So far, applying acoustic on measuring sea ice thickness has been proved as a feasible method in a laboratory environment. Due to weather and equipment reasons, a field test has not been done yet. In a natural environment, there may be some factors that the author did not take into account. Therefore, in the next stage, this whole system should be tested in an Arctic area to achieve several objectives including: finding out whether all hardware parts can work normally in a low temperature (the lowest temperature of the cold room can be set as -20°C, but in a natural environment it may be lower than -40°C); finding out how many transducers placed at different locations are needed to obtain reliable results (10 transducers that can collect data from 34 locations are good enough in a lab experiment, but in natural environment it may require more due to poorer sea ice conditions); and observing the features of the bottom surface of real first year sea ice and then adjusting algorithm parameters. Furthermore, to protect the sensor system from any damage caused by the external environment and maintain its inside working temperature, an isolated and sealed enclosure should be applied.

In addition, wavelet transform is another new technology applied in signal processing in recent decades. Similar with FT to change the signal to a set of sinusoids, it decompose the signal to a family of wavelets that have different time-widths adapted to their frequencies [25]. Compare with FT, which is only localized in frequency, this method can capture both frequency and time information. For higher frequencies, wavelets uses shorter windows to provide better time resolution than the STFT which uses fixed window over all signal. Therefore, in the future, as the collected signal becoming more complicated in real environment, replacing the SFTF by a wavelet transform will improve the experimental results.

Bibliography

[1] D. Claude and B. Colburne, "Course notes of arctic ocean enigeering." Memorial University, 2014.

[2] `http://nca2014.globalchange.gov/report/our-changing-climate/melting-ice#intro-section-2`.

[3] J. C. Comiso, C. L. Parkinson, R. Gersten, and L. Stock, "Accelerated decline in the arctic sea ice cover," *Geophysical research letters*, vol. 35, no. 1, 2008.

[4] D. Fissel, J. Marko, and H. Melling, "Upward looking ice profiler sonar instruments for ice thickness and topography measurements," in *OCEANS'04. MTTS/IEEE TECHNO-OCEAN'04*, vol. 3, pp. 1638–1643, IEEE, 2004.

[5] C. Haas, "Evaluation of ship-based electromagnetic-inductive thickness measurements of summer sea-ice in the bellingshausen and amundsen seas, antarctica," *Cold Regions Science and Technology*, vol. 27, no. 1, pp. 1–16, 1998.

[6] A. Pfaffling, "Helicopter electromagnetic sea ice thickness estimation: an induction method in the centimetre scale= meereisdickenbestimmung mittels hubschrauberelektromagnetik: ein induktionsverfahren im zentimeterbereich," *Berichte zur Polar-und Meeresforschung (Reports on Polar and Marine Research)*, vol. 553, 2007.

[7] https://www.nde-ed.org/EducationResources/CommunityCollege/Ultrasonics/Introduction/description.htm.

[8] http://polar.erdc.dren.mil/people/personnel_sid/perovichweb/HotraxWeb/arctic_basin/field2005/to_the_pole.html.

[9] https://www.polartrec.com/expeditions/oden-antarctic-expedition-2010/journals/2010-12-17.

[10] https://www.olympus-ims.com/data/File/panametrics/UT-technotes.en.pdf.

[11] http://www.acousticsunpacked.org/AcousticBackground/AcousticTransducers.html.

[12] http://www.optel.eu/manual/english/opbox21.html.

[13] https://developer.mbed.org/platforms/mbed-LPC1768/.

[14] http://uk.farnell.com/omron-electronic-components/g5v-2-24dc/relay-signal-dpdt-30vdc-2a/dp/9949500.

[15] https://ireneviguegux.wordpress.com/2017/02/06/understanding-the-fourier-transform/.

[16] http://sethares.engr.wisc.edu/vocoders/phasevocoder.html.

[17] T. Bell, R. Briggs, R. Bachmayer, and S. Li, "Augmenting inuit knowledge for safe sea-ice travel—the smartice information system," in *2014 Oceans-St. John's*, pp. 1–9, IEEE, 2014.

[18] J. Hyatt, M. Visbeck, R. C. Beardsley, and W. B. Owens, "Estimating sea-ice coverage, draft, and velocity in marguerite bay (antarctica) using a subsurface

moored upward-looking acoustic doppler current profiler (adcp)," *Deep Sea Research Part II: Topical Studies in Oceanography*, vol. 55, no. 3, pp. 351–364, 2008.

[19] A. Kovacs and R. M. Morey, "Sounding sea ice thickness using a portable electromagnetic induction instrument," *Geophysics*, vol. 56, no. 12, pp. 1992–1998, 1991.

[20] `http://worldoceanreview.com/en/wor-1/climate-system/great-ocean-currents/`.

[21] M. E. Shokr and N. K. Sinha, "Arctic sea ice microstructure observations relevant to microwave scattering," *Arctic*, pp. 265–279, 1994.

[22] Q. Shen, M. Omar, and S. Dongri, "Ultrasonic nde techniques for impact damage inspection on cfrp laminates," *Journal of materials science research*, vol. 1, no. 1, p. 2, 2012.

[23] N. Netshidavhini and B. M. Raymond, "Effects of various couplants on carbon steel and aluminium materials using ultrasonic testing," in *18th World Conference on Nondestructive Testing*, pp. 16–20, 2012.

[24] Y. Quan and J. M. Harris, "Seismic attenuation tomography using the frequency shift method," *Geophysics*, vol. 62, no. 3, pp. 895–905, 1997.

[25] M. Sifuzzaman, M. Islam, and M. Ali, "Application of wavelet transform and its advantages compared to fourier transform," 2009.

Appendix A.

Matlab Code

Import data to Matlab

```
clc
clear all

highsamples=[];

baseDir='.\20151211UnknownThick\HighTrig\';
contains=dir(baseDir);

for k=1:length(contains)
    if (contains(k).isdir)
        continue;
    end
    disp(contains(k).name);
    fid=fopen([baseDir contains(k).name],'r');
    x=fread(fid,35000,'uint8');
```

```
    y=(x-128)/1.28;
    highsamples=[highsamples,y];
    fclose(fid);
end
highsamples=highsamples'; //save all data into highsamples.mat
                          //which is readable for Matlab
```

Algorithm used to extract final result

```
clc
clear
Fs=100*1000*1000;
load highsamples.mat;  //Import data package
load Hd250.mat; //Import filter

[testNum testLength]=size( highsamples);
for m=4:testNum
    realdata= highsamples(m,:);
    y=realdata-mean(realdata);
    figure;plot(y);
    title('Original signal')
    ylabel('Voltage');
    xlabel('Sampling points')
    axis([0,35000,-100,100]);

y=filter(Hd250,y);
   figure;plot(y);
```

```
    title('Filtered signal')
    ylabel('Voltage');
    xlabel('Sampling points')
    axis([0,35000,-100,100]);


[S,F,T,P] = spectrogram(y,hamming(512),500,2048,Fs,'yaxis');
     figure;
     surf(T,F,P);
     view(2);
     axis([0 35e-5 0 0.7e6]);
     title('Frequency spectrum')
     ylabel('Frequency');
     xlabel('Time(s)')

maxpower=max(P);
powersize=length(maxpower);

     for i=1:powersize
               index=find(P(:,i)==maxpower(i));
               if(index<5||index>7)
               P(:,i)=0;
               end
     end

power=sum(P(5:end,:));
```

```
    figure;
    plot(T,power);
    title('Power curve');
    xlabel('Time(s)');
    ylabel('Power density(W/Hz)');

[pks,locs]=findpeaks(power,'minpeakheight',0.001*max(power) );

locmax=locs(find(power(locs)==max(power(locs))));

locs=locs(find(locs>20));
locs=locs(find(locs<length(power)-20));

DeletNum1=[];
[x y]=size(locs);
for a=1:y
    if(power(locs(a)-20)==0power(locs(a)+20)==0)
        DeletNum1=[DeletNum1,locs(a)];
    end
end

[s t]=size(DeletNum1);
for n=1:t
    temp1=find(locs==DeletNum1(n));
    locs(temp1)=[];
end
```

```
trough=find(diff(sign(diff(power)))>0)+1;

[e f]=size(locs);
DeletNum=[];

for a=2:f-1
    smalltrough=trough(find(trough<locs(a)));
    lowBound=max(smalltrough);
    largetrough=trough(find(trough>locs(a)));
    highBound=min(largetrough);
    lowDif=power(locs(a))-power(lowBound);
    highDif=power(locs(a))-power(highBound);
    if(lowDif<0.3*power(locs(a))||highDif<0.3*power(locs(a)))
    DeletNum=[DeletNum,locs(a)];
    end
end

    l=length(DeletNum);
    tooNear=[];
        for n=1:l-1
         temp1=DeletNum(n+1)-DeletNum(n);
            if(temp1<=50)
            if power(DeletNum(n+1))>=power(DeletNum(n))
               tooNear=[tooNear,DeletNum(n+1)];
             else
```

```
                tooNear=[tooNear,DeletNum(n)];
            end
        end

    end

    l2=length(tooNear);
        for o=1:l2
            temp2=find(DeletNum==tooNear(o));
            DeletNum(temp2)=[];
        end


[s t]=size(DeletNum);
for n=1:t
    temp3=find(locs==DeletNum(n));
    locs(temp3)=[];
end

[x y]=size(locs);
DeletNum2=[];
for a=1:y-1
    if(locs(a+1)-locs(a)<=50)
        if(power(locs(a+1))>power(locs(a)))
            DeletNum2=[DeletNum2,locs(a)];
        else
```

```
                DeletNum2=[DeletNum2,locs(a+1)];
            end
        end
end

[s t]=size(DeletNum2);
for n=1:t
    temp4=find(locs==DeletNum2(n));
    locs(temp4)=[];
end

[x y]=size(locs);
  for a=2:y
      peak=locs(a);

      reflectstatic1(m,peak-20:peak+20)=1;

  end

end

[i j]=size(reflectstatic1);
 figure;plot(T(1:j),sum(reflectstatic1(:,1:j)) );
 title('Final Result of 16cm Sea Ice');
 xlabel('Time(s)');
 ylabel('Amount of valid reflections');
```

Appendix B.

C/C++ Code

Main program used to control OPBOX and mbed

```
#include "wrap_opbox21f.h"
#include <stdio.h>
#include <conio.h>
#include <math.h>
#include <windows.h>
#include <string.h>
#include"WTYPES.H"

int CheckNr(int check)
{
        if(check>=0)
                return 0;

        else
                return 1;
```

```
}


int main()
{
        unsigned short Info1,Info2;
        char vers[50];
        int status, temp;
        int i=0;
        int frame_cnt;
        int check=0;
        int n = 0;
        int Test_NumLow = 0;
        int Test_NumHigh = 0;
        unsigned char *data;
        char buffer_TGC_DAC[35000] = {0};
        const char *com[2] = { "OK \n", "Not OK \n" };
        SYSTEMTIME time;
        boolean Trigger_Time;
        printf("Initialization %d \n", op_wrp_Im_data());
        op_wrp_OpenOpbox();    // Connect to Opbox
    while (Test_NumLow <= 100)
        {
    op_wrp_Im_data();     // Initialize data
        op_wrp_Instr_Restet();  // Reset OPbox
    op_wrp_PowerOnOff(1);    // Turn on DC_DC and Analog filter
```

```
        op_wrp_Instr_RestetFIFO();    // Reset FIFO
        data = op_wrp_GetDataHandle();
        Sleep(1000);

        GetSystemTime(&time);
        int month = time.wMonth;
        int date = time.wDay;
        int hour = time.wHour;
        int min = time.wMinute;
        printf("Current time is %d%d \n", hour, min);

 Trigger_Time = (hour == 12 || hour==15||
                 ||hour == 18 || hour == 21);
 printf("Trigger_Time is %d \n", Trigger_Time);

 if (Trigger_Time == 1)
{
 data = op_wrp_GetDataHandle();
 check = op_wrp_GetFrame_Cnt();
 printf("Lowest Trigger Level How many
 frames are ready to read: %d \n", check);

 check = op_wrp_GetFrame_Idx();
 printf("Lowest Trigger Level Current
 frame is ready to read: %d \n", check);
```

```
op_wrp_SetGainMode(1);
op_wrp_TrigEnable(0);

for (int i = 0; i < 35000; i++)  //Set up TCG Gain
{
float itemp = i;
itemp = 44 * i / 35000;
buffer_TGC_DAC[i] = 90+floor(itemp);
                                        }

op_wrp_DoDAC(buffer_TGC_DAC,35000);
op_wrp_TrigEnable(1);    // Enable trigger
op_wrp_SetAmplitude(30);     // Set trigger level
Sleep(200);
op_wrp_SetPulserTime(35, 0);     // Set pulse time
Sleep(200);
check = op_wrp_GetPulserTime(&status, &temp);
printf("Lowest Trigger Level Pulser duration is %d,
status is %d \n", status, temp);
op_wrp_SetAnalogFilter(1);     // Set analog filter
Sleep(200);
op_wrp_SetPreAmp(1);    // Set pre-amplifier
Sleep(200);
op_wrp_SetSamplingFreq(100.0);     // Set sampling frequency
Sleep(200);
```

```
op_wrp_SetDataMode(0);     // Set data mode as raw data
Sleep(200);
op_wrp_SetSource(0);       // Set mode as TT    0–TT 1–PE
Sleep(200);
op_wrp_SetDelay(0);     // Set delay as 0us
Sleep(200);
op_wrp_SetDepth(35000);     // Set window size 100us
check = op_wrp_GetDepth();
printf("Lowest Trigger Level Depth is %d \n", check);
Sleep(200);
op_wrp_SetPacket_Len(1);
op_wrp_SetTriggerSource(3);     // turn on trigger

for (i = 0; i < 100000; i++)
{
      check = op_wrp_Check_Frame_Ready();
      if (check == 1)
      {
      printf("Lowest Trigger Level Data is ready to read.\n");
      break;
      }
      else{
      printf("Lowest Trigger Level Data is not ready to read.\n");
            }
            }
```

```
    frame_cnt = op_wrp_GetFrame_Cnt();
    printf("Lowest Trigger Level
    How many frames are ready to read: %d \n", check);

    check = op_wrp_GetFrame_Idx();
    printf("Lowest Trigger Level
    Current frame is ready to read: %d \n", check);

check = op_wrp_GetData(35054* frame_cnt);
    printf("Lowest Trigger Level Get Data %d \n", check);

FILE *fp;

    char datafilename[100];
sprintf(datafilename, "C:\\Users\\lishu_000\\Desktop
\\Checking\\201512112UnknownThick\\lowflower%d.txt",
 Test_NumLow);

    fp = fopen(datafilename, "w");     // creat data file

    for (int t = 54; t <= 35053; t++)
    {
    fprintf(fp, "%c", data[t]);
}
    fclose(fp);
    frame_cnt = op_wrp_GetFrame_Cnt();
```

```
        op_wrp_Free_data();
        Sleep(1000);
    Test_NumLow = Test_NumLow + 1;
    }

// Highest Level Trigger

    op_wrp_Im_data();      // Initialize data
    op_wrp_Instr_Restet();  // Reset OPbox
    op_wrp_PowerOnOff(1);    // Turn on DC_DC and Analog
        op_wrp_Instr_RestetFIFO();    // Reset FIFO
        Sleep(1000);
        GetSystemTime(&time);
        printf("Current time is %d%d \n", hour, min);
    Trigger_Time = (hour == 12 || hour == 15 ||
                    hour == 18 || hour == 21);
        printf("Trigger_Time is %d \n", Trigger_Time);

        if (Trigger_Time == 1)
        {
        data = op_wrp_GetDataHandle();
        check = op_wrp_GetFrame_Cnt();
        printf("Highest Trigger Level How many frames
                are ready to read: %d \n", check);

        check = op_wrp_GetFrame_Idx();
```

```
printf("Highest Trigger Level Current frame
        is ready to read: %d \n", check);

op_wrp_SetGainMode(1);
printf("After setup gain mode \n" );
op_wrp_TrigEnable(0);
printf("After setup TrigEnable \n");

for (int i = 0; i < 35000; i++)
{
float itemp = i;
itemp = 44 * i / 35000;
buffer_TGC_DAC[i] = 90 + floor(itemp);
}

op_wrp_DoDAC(buffer_TGC_DAC, 35000);
printf("After setup TGC_DAC \n");

op_wrp_TrigEnable(1);    // Enable trigger
printf("before setup all parameters \n");
op_wrp_SetAmplitude(63);     // Set trigger level
printf("After setup Amplitude \n");
Sleep(200);

op_wrp_SetPulserTime(35, 0);     // Set pulse time
printf("After setup Pulser Time \n");
```

```
Sleep(200);

check = op_wrp_GetPulserTime(&status, &temp);
printf("Highest Trigger Level Pulser duration is %d,
        status is %d \n", status, temp);
op_wrp_SetAnalogFilter(1);     // Set analog filter
                               //as 0.5-25Mhz
printf("After setup filter \n");
Sleep(200);

op_wrp_SetPreAmp(1);    // Set pre-amplifier
printf("After setup PreAmp \n");
Sleep(200);

op_wrp_SetSamplingFreq(100.0);     // Set sampling frequency
                                   //as 100Mhz
printf("After setup SmpFreq \n");
Sleep(200);

op_wrp_SetDataMode(0);     // Set data mode as raw data
printf("After setup data mode \n");
Sleep(200);

op_wrp_SetSource(0);      // Set mode as TT
printf("After setup source \n");
Sleep(200);
```

```
    op_wrp_SetDelay(0);     // Set delay as 0us
    printf("After setup delay \n");
    Sleep(200);

    op_wrp_SetDepth(35000);     // Set window size 100us
    printf("After setup depth \n");
    Sleep(200);

    check = op_wrp_GetDepth();
    printf("Highest Trigger Level Depth is %d \n", check);
    op_wrp_SetPacket_Len(1);
    op_wrp_SetTriggerSource(3);     // turn on trigger


    for (i = 0; i < 100000; i++)
{
    check = op_wrp_Check_Frame_Ready();
    if (check == 1)
    {
    printf("Highest Trigger Level Data is ready to read.\n");
    break;
    }
    else{
    printf("Highest Trigger Level Data is not ready to read.\n");
    }
```

```
    }

    frame_cnt = op_wrp_GetFrame_Cnt();
    printf("Highest Trigger Level How many frames
           are ready to read: %d \n", check);

    check = op_wrp_GetFrame_Idx();
    printf("Highest Trigger Level Current frame
            is ready to read: %d \n", check);
Sleep(3000);

    check = op_wrp_GetData(35054 * frame_cnt);
    printf("Highest Trigger Level Get Data %d \n", check);

    FILE *fp;
char datafilename[100];
sprintf(datafilename, "C:\\Users\\lishu_000\\Desktop\\Checking
\\201512112UnknownThick\\highflower%d.txt", Test_NumHigh);

    fp = fopen(datafilename, "w");    // creat data file
    for (int t = 54; t <= 35053; t++)
    {
 fprintf(fp, "%c", data[t]);
}
    fclose(fp);
    frame_cnt = op_wrp_GetFrame_Cnt();
```

```
        printf("Highest Trigger Level How many frames
                are ready to read: %d \n", check);
        op_wrp_Free_data();
    Sleep(1000);

        Test_NumHigh = Test_NumHigh + 1;
        printf("Current test %d is done \n", Test_NumHigh - 1);

        getch();
    }

}
system("pause");
return 0;
}

 #include "mbed.h"
Serial pc(USBTX,USBRX);
char c;
Digitalout relay1(p13);
Digitalout relay2(p14);
Digitalout relay3(p15);
Digitalout relay4(p16);
Digitalout relay5(p30);
Digitalout relay6(p29);
Digitalout relay7(p28);
```

```
Digitalout relay8(p27);
Digitalout myled(LED1);

int main(){
while(1){
if(pc.getc()==0x37){
relay1=0; //open switch1
relay2=0;
relay3=0;
relay4=0;
relay5=0;
relay6=0;
relay7=0;
relay8=0;

wait(2);
relay1=1; //close switch1, transducer cuircuit start work.
relay4=1;

wait(5);
relay1=0;
relay4=0;
relay2=1;
relay3=1;

wait(5);
```

```
relay2=0;
relay3=0;
relay5=1;
relay8=1;

wait(5);
relay5=0;
relay8=0;
relay6=1;
relay7=1;

wait(5);
relay6=0;
relay7=0;
printf("Channel changing finished \n");
}
}
}
```